Chemically and Thermally Activated Decomposition of Secondary Butyl Radical

Vadim D. Knyazev*,†,‡ and Wing Tsang‡

Department of Chemistry, The Catholic University of America, Washington, D.C. 20064, and National Institute of Standards and Technology, Physical and Chemical Properties Division, Gaithersburg, Maryland 20899

Received: May 24, 2000; In Final Form: September 14, 2000

Experimental literature data on the chemically and thermally activated decomposition of *sec*-C_4H_9 radical were analyzed by weak collision master equation modeling. A reaction model with very little flexibility in its properties was created on the basis of ab initio calculations and experimental kinetic and thermochemical data. Rate constants and branching fractions for the chemically activated reaction were calculated using the *virtual component* formalism. The resultant model quantitatively describes (1) data on the stabilization-to-decomposition ratios as functions of temperature and pressure obtained in experiments using H + butene reactions as the sources of chemical activation and (2) experimental data on the thermal decomposition of *sec*-C_4H_9 radicals. Values of $\langle\Delta E\rangle_{down}$, the average energy transferred per deactivating collision, derived from modeling of experimental data demonstrate strong positive temperature dependencies for a variety of bath gases. Qualitative shapes of falloff curves for the chemically activated reaction were analyzed. Comparison of the weak collision model with the results of the modified strong collision treatment demonstrates the inadequacy of the latter.

I. Introduction

Modeling of elementary unimolecular reactions has become a powerful tool of chemical kinetics. Such modeling presents the only way to extrapolate experimental pressure and temperature dependent data on reaction rate constants and channel branching fractions to conditions outside of the experimental ranges. Currently, statistical theories of unimolecular reactions are routinely used to fit experimental data and to predict kinetic parameters under experimentally inaccessible conditions. In such fitting exercises, typically one or several parameters of a model are adjusted to reproduce experimental data. Usually, models of unimolecular reactions have substantial flexibility due to having a number of parameters that are unknown or known with insufficient accuracy and thus need to be determined from fitting of experimental data. Such parameters necessarily include properties of collisional energy transfer (such as $\langle\Delta E\rangle_{down}$, the average energy transferred per deactivating collision, and its temperature dependence), the entropy of the transition state (often expressed via the preexponential factor), and the reaction barrier height. If a chemically activated unimolecular reaction is considered, model flexibility increases since two or more transition states are involved. Such flexibility makes unimolecular reaction modeling vulnerable to criticism because it obscures the borderline between a simulation based on rigorous understanding of physical reality and a simple multiparameter fitting exercise.

One way of improving the reliability of simulation is to reduce the flexibility of the model by determining critical transition state properties with a higher degree of accuracy via methods other than fitting pressure-dependent experimental data. This can be done, for example, by applying quantum chemistry techniques to determine those properties that can be accurately obtained in such calculations (e.g., geometrical parameters, most of vibrational frequencies) and then fitting the most critical transition state parameters to reproduce high-pressure-limit rate constant temperature dependencies, if these are known from experiment. Such a procedure, at a minimum, ensures that the energy dependence of the product of the density-of-states function ($\rho(E)$) and the microscopic energy-dependent rate constants ($k(E)$) is determined accurately within the relevant range of energies, as there is a unique correspondence between the $\rho(E)$ $k(E)$ function on one hand, and temperature-dependent rate constants $k(T)$, on the other ($k(T)$ is obtained by a Laplace transform of $\rho(E)$ $k(E)$).[1−3]

If the number of model properties that need to be determined from fitting experimental pressure-dependent data is thus reduced to just a few parameters, then a quantitative comparison of model predictions with extensive sets of pressure-dependent experimental data provides an opportunity to test the adequacy of the underlying theory. In particular, it is interesting to test the adequacy of the description of a competition between unimolecular reaction and collisional energy transfer, which determines experimentally observed pressure dependencies.

In general, testing collisional energy transfer models for reaction rate simulation purposes is difficult since rate constant pressure dependencies (falloff) are, typically, spread over wide pressure ranges. Very few sets of experimental data that cover the entire pressure range between the low-pressure and the high-pressure limits are available in the literature. Attempts at evaluating the performance of theory by matching the calculated and experimental falloff shapes are, therefore, hindered by limited availability of experimental data. Even those few experimental falloff shapes that are available are, typically, restricted to low and intermediate temperature measurements where the shape of the rate constant pressure dependence is determined by an interplay of energy-dependent reaction and collisional energy transfer within a relatively narrow interval of energies around the reaction barrier. Thus, even in the best case, only properties of collisional energy transfer at the energy of the barrier can be evaluated from modeling of such reaction rates.

* Corresponding author. E-mail: knyazev@cua.edu.
† The Catholic University of America.
‡ National Institute of Standards and Technology.

10.1021/jp001921z CCC: $19.00
Published on Web 10/21/2000

A different, more stringent test can be applied to statistical theories of unimolecular reactions and collisional energy transfer models by attempting to reproduce experimental rate data obtained experimentally for the same reaction but with qualitatively different shapes of energy distributions. Reactions that are activated chemically through channels with different energy barriers or activated chemically in one case and thermally in the other case provide such an opportunity.

In the current work, we perform a simulation of two reactive systems involving the same elementary unimolecular reaction, the decomposition of secondary butyl radical, but characterized by different methods of activation. In the case of chemical activation, highly vibrationally excited *sec*-C_4H_9 radicals are formed in thermal reactions by addition of hydrogen atoms to double bonds of three different isomers of butene. In the thermal activation case, thermalized radicals are excited to energies required for reaction by activating collisions with the bath gas. The reaction model created in this work has very little flexibility in its parameters, which allows us to concentrate on properties of collisional energy transfer. Simulation successfully reproduces experimental data on both chemically and thermally activated processes. Experimental data on the chemically activated reactions are those of Rabinovitch and co-workers,[4−11] and rate constants of thermally activated *sec*-C_4H_9 decomposition are taken from Knyazev et al.[12]

The article is organized as follows. Section I is an introduction. Section II describes the model of secondary butyl radical decomposition, which includes four different product channels, three of those being also used (in the reverse direction) as chemical activation sources. First, experimental data are reviewed (subsection II.1). Second, critical properties of transition states are determined by ab initio calculations and by fitting experimental data on the high-pressure-limit rate constants obtained from the literature (subsection II.2). Third, solution of the master equation describing the interplay of collisional activation/deactivation (weak collision model) and unimolecular reaction is used within the *virtual components* formalism[13] to reproduce the experimental data (subsection II.3). A discussion is presented in section III.

II. Model

II.1. Reaction Systems and Experimental Data. *Chemically Activated Reactions.* All experimental data on the chemically activated decomposition of secondary butyl radical come from the work of Rabinovitch and co-workers.[4−11] To a large extent, these pioneering studies (the experimental part and equally important theoretical work, also see refs 14, 15, and references therein) conducted in late 1950s and early 1960s formed the foundation of modern understanding of chemically activated processes. In the experiments, H atoms produced in a discharge were allowed to effuse through an injector into the center of a reactor containing butene gas or its mixtures with other bath gases. Final products were analyzed by gas chromatography and experimental ratios of stabilization to decomposition rates were thus obtained. The sequence of processes occurring in such a system can be represented by the following scheme:

$$\mathrm{H} + \mathrm{C_4H_8} \underset{-1a}{\overset{1a}{\leftrightarrow}} \textit{sec}\text{-}\mathrm{C_4H_9}^* \xrightarrow{1b} \mathrm{CH_3} + \mathrm{C_3H_6}$$

$$\xrightarrow[(+\mathrm{M})]{1c} \textit{sec}\text{-}\mathrm{C_4H_9} \qquad (1)$$

Reaction 1a forms highly vibrationally excited secondary butyl radicals that can undergo back decomposition to reactants (−1a), further reactions via channel 1b, or stabilization by collisions with the bath gas (1c). Three different isomers of butene (*cis*-C_4H_8, *trans*-C_4H_8, and 1-C_4H_8) were used by Rabinovitch and co-workers to form excited *sec*-C_4H_9 radicals in reaction 1a. All of them are considered in the current work. Out of all three possible H + butene reactions, the H + *cis*-C_4H_8 system was studied by Rabinovitch and co-workers most extensively and, therefore, it is paid most attention here.

A full reaction scheme should also include other possible decomposition channels of excited butyl radicals in addition to channel 1b, such as those forming H atoms and other butene isomers. However, the contributions of these other channels were negligible under all experimental conditions (due to higher barriers) and thus they are not shown in (1).

The experiments of Rabinovitch et al. were conducted at four temperatures: 170, 195, 298, and 373 K, and at pressures from 0.52 to 1307 Pa (3.9×10^{-3} − 9.8 Torr). Data obtained at the high end of the pressure range (>13 Pa or 0.1 Torr) appear to be most reliable since the low-pressure results were affected[7−10] by the "low-pressure artifact" or the appearance of stabilization products that could not be explained within the kinetic mechanism assumed by the authors in their data analysis. The authors corrected some of their low-pressure data to account for this artifact. However, since the effect has an unknown origin, the correction was phenomenological in nature (estimated by extrapolation: amounts of *n*-butane formed in the limit of low pressures were subtracted from the experimental yields of *n*-butane obtained at higher pressures) and thus can be considered only as approximate.

The experiments of Rabinovitch et al. included studies of reactions of H with deuterated butenes and of deuterium atoms with butenes and deuterated butenes. Results of these experiments with deuterated species are not considered in the current work since the presence of D atoms significantly changes the effective potential energy surface (via changes in the zero-point vibrational energy, ZPVE) and the tunneling probabilities. Such changes in the reaction model due to substitution of D for H are not easily accounted for because of the limited accuracy of knowledge of vibrational frequencies and associated force constants. For example, a quite plausible error in a transition state ZPVE by 100 cm^{-1} (1.2 kJ mol^{-1}) will result in a change in a room-temperature rate constant by as much as 62%. Thus, treatment of reactions of deuterated species is not attempted here in order to avoid additional sources of errors in the model.

Many of the experiments of Rabinovitch et al. were conducted using the corresponding butene as bath gas. However, the work of Kohlmaier and Rabinovitch[9,10] included experimental studies of reaction 1 in a variety of bath gases, which included noble (He, Ar, Ne, Kr), diatomic (N_2, H_2, D_2) and polyatomic (C_4H_8, CO_2, SF_6, CH_4, CH_3Cl, CD_3F) gases. Most of the detailed experimental data of Rabinovitch and co-workers were published in dissertations of Harrington,[6] Kubin,[8] and Kohlmaier.[10] Journal articles 5, 7, 9, and 11 presented most of the data in plots in mathematically transformed form with only selected examples of original experimental results given in tables.

Thermally Activated Reaction. The thermal decomposition of secondary butyl radicals

$$\textit{sec}\text{-}\mathrm{C_4H_9} \rightarrow \mathrm{CH_3} + \mathrm{C_3H_6} \qquad (2)$$

was studied experimentally by Knyazev et al.[12] Experiments were conducted in a heatable flow reactor by the Laser Photolysis/Photoionization Mass Spectrometry method. Secondary butyl radicals were obtained by laser photolysis of a molecular precursor, thermalized by collisions with the bath gas, and their unimolecular decomposition was monitored in real

time at temperatures between 598 and 680 K and at bath gas densities $(3-18) \times 10^{16}$ molecules cm^{-3}. Three bath gases: He, Ar, and N_2 were used in the experiments. Low initial radical concentrations ($\leq 10^{11}$ molecules cm^{-3}) used allowed the authors to isolate the reaction under study and avoid potential influence from side reactions (such as radical−radical processes). The authors applied master equation/RRKM[1−3] modeling with analysis of literature data on the high-pressure-limit rates of the direct and the reverse reactions to reproduce and extrapolate their experimental data to experimentally inaccessible conditions.

Literature Data on High-Pressure-Limit Reaction Rate Constants of Individual Channels of Decomposition and Formation of Secondary Butyl Radical. Reactions 1 and 2 (including all isomeric versions of reaction 1) involve four transition states: those for H atom addition to three isomers of butene,

$$H + cis\text{-}C_4H_8 \leftrightarrow sec\text{-}C_4H_9 \qquad (1ac,-1ac)$$

$$H + trans\text{-}C_4H_8 \leftrightarrow sec\text{-}C_4H_9 \qquad (1at,-1at)$$

$$H + 1\text{-}C_4H_8 \leftrightarrow sec\text{-}C_4H_9 \qquad (1a\alpha,-1a\alpha)$$

and the transition state for the decomposition of *sec*-butyl radical to CH_3 and C_3H_6:

$$sec\text{-}C_4H_9 \leftrightarrow CH_3 + C_3H_6 \qquad (1b,-1b)$$

Here, symbols "c", "t", and "α" in reaction numbers stand for cis-, trans-, and α-butene (1-butene), respectively.

Temperature dependencies of the high-pressure-limit rate constants of reactions 1ac, 1at, and 1aα have been determined experimentally by Harris and Pitts[16] and Kyogoku et al.[17] Harris and Pitts used flash photolysis to produce and resonance fluorescence to detect H atoms. These authors worked in the 298−445 K temperature range at pressures 6.7−13.3 kPa (50−100 Torr). Kyogoku et al. applied the pulsed electron radiolysis/Lyman-α absorption technique to study the same reactions at $T = 200-500$ K and 80 kPa (600 Torr). The rate constant values of Kyogoku et al. are somewhat higher that those of Harris and Pitts, the disagreement being more pronounced at lower temperatures (e.g., a factor of 1.37 at 298 K for reaction 1ac). A similar disagreement between the results of refs 16 and 17 is observed for the reaction of H atoms with the fourth isomer of butene, *iso*-C_4H_8:

$$H + iso\text{-}C_4H_8 \rightarrow t\text{-}C_4H_9 \qquad (1ai)$$

For reaction 1ai, good agreement exists between the results of Harris and Pitts[16] and the earlier measurements of Canosa et al.[18] (See ref 19 for a brief discussion.) Also, recent measurements of Bryukov et al.[20] (discharge flow/resonance fluorescence method, $T = 299-505$ K) agreed with the data of Harris and Pitts on the H + *iso*-C_4H_8 reaction. Considering the high sensitivity of the resonance fluorescence method to H atom detection and the agreement between the results of ref 16 with other literature data on reaction 1ai, we adopt the results of Harris and Pitts (Table 1) as the most accurate measure of the high-pressure-limit rate constants of reactions 1ac, 1at, and 1aα.

Experimental information on the high-pressure-limit rate constants of reaction (1b,−1b) include data on both the direct (Lin and Laidler,[34] Gruver and Calvert)[35] and reverse (Miyoshi and Brinton,[31] Cvetanovic and Irwin,[32] Tedder et al.,[36] and Baldwin et al.)[33] reactions. Detailed discussion of these works can be found in ref 12. We follow the analysis of Knyazev et al.[12] and take the combined results of Miyoshi and Brinton[31] and Cvetanovic and Irwin[32] (which are in perfect agreement with each other after correction for an erroneously reported preexponential factor in ref 31, see refs 33 and 12) as the basis for analysis of reaction 1b transition state properties. These two studies together give

$$k^{\infty}_{-1b} = 1.81 \times 10^{-12} \exp(-4239\ \mathrm{K}/T)\ \mathrm{cm^3\ molecule^{-1}\ s^{-1}} \qquad (I)$$

for the high-pressure-limit rate constant temperature dependence at $T = 353-453$ K.

Thermochemistry of Involved Species. The most direct determination of the heat of formation of secondary butyl radical is that of Seakins et al.[37] These authors used experimental data on the *sec*-C_4H_9 + HBr ↔ Br + *n*-C_4H_{10} reaction kinetics to obtain $\Delta_f H^o_{298}(sec\text{-}C_4H_9) = 67.5 \pm 2.3$ kJ mol^{-1} from a third law analysis and $\Delta_f H^o_{298}(sec\text{-}C_4H_9) = 67.6 \pm 3.0$ kJ mol^{-1} from a second law treatment. Their results agree within experimental uncertainties with the value obtained by Knyazev et al.[12] (65.0 ± 3.4 kJ mol^{-1}) in their analysis of the unimolecular decomposition of *sec*-butyl radical, reaction 1b. We select for further use the third-law value of Seakins et al. The influence of the enthalpy of formation of *sec*-C_4H_9 on the results of modeling and the final recommended (slightly adjusted) value are discussed in subsection II.3.

Standard enthalpies of formation of other species are taken from ref 24 (H, 217.994 kJ mol^{-1}), 38 (C_3H_6, 20.0 ± 0.8 kJ mol^{-1}), 39 (*cis*-C_4H_8, −7.1 ± 1.0 kJ mol^{-1}; *trans*-C_4H_8, −11.4 ± 1.0 kJ mol^{-1}; 1-C_4H_8, 0.1 ± 1.0 kJ mol^{-1}), 40, and 41 (CH_3, 146.0 ± 1.0 kJ mol^{-1}).

Experimental values of vibrational frequencies and rotational constants of secondary butyl radical are not available. The results of Chen et al.[21] on the frequencies, geometry, and torsional barriers of *sec*-C_4H_9 obtained in ab initio calculations were used for the model. Properties of CH_3 and C_3H_6 were taken from refs 24 and 25, respectively. Vibrational frequencies, geometries, and torsional barriers of the three butene isomers involved were taken from Zakharieva-Pencheva and Förster,[22] Durig,[28] Engeln and Reuss,[29] Durig and Compton,[23] Kondo et al.,[26] and Murcko et al.[27] All molecular properties of the involved species are listed in Table 1.

II.2. Properties of Transition States. Properties of transition states are of critical importance to the model. Methods of quantum chemistry that can be applied to the current reactive system cannot be expected to produce sufficiently accurate values of energy barriers and low value vibrational frequencies. Therefore, in the current work, an approach based on a combination of ab initio computations and fitting of high-pressure-limit rate data was used. First, those properties of transition states for which quantum chemical methods can be expected to yield accuracy sufficient for chemical modeling were obtained in ab initio calculations. These properties include geometries, barriers for internal rotations (torsions), and "widths" of the barriers (the "width" parameter to be used in calculation of tunneling probabilities, vide infra). Second, vibrational frequencies of the transition states were calculated and scaled by 0.8929.[42] Finally, the temperature dependencies ($k^{\infty}(T)$) of the high-pressure-limit rate constants were calculated for reactions 1ac, 1at, 1aα, and −1b and the values of the reaction barrier heights and the lowest vibrational frequencies of the transition states were adjusted to reproduce the experimental $k^{\infty}(T)$ dependencies. The resultant final properties of the transition states are listed in Table 1.

Geometry optimization and frequency calculations were performed at the UHF/6-31G(d) level and energies of torsional barriers were calculated at both UHF/6-31G(d,p) and UMP2/

TABLE 1: Properties of Molecules and Elementary Reactions Used in the Model.

Vibrational Frequencies (cm^{-1}, Scaled Unadjusted ab Initio Values in Brackets if Different):

$CH_3\cdots CH_2CHCH_3^{\ddagger}$	123 [126], 180 [247], 392, 496, 524, 617, 777, 846, 876, 934, 936, 1008, 1142, 1190, 1369, 1401, 1405, 1406, 1452, 1462, 1488, 2840, 2881, 2909, 2912, 2963, 2970, 3036, 3039, 3044
$H\cdots cis\text{-}C_4H_8^{\ddagger}$	365 [253], 400 [271], 406, 437, 542, 683, 800, 909, 939, 994, 1017, 1026, 1123, 1203, 1361, 1401, 1412, 1440, 1455, 1463, 1467, 1495, 2848, 2855, 2887, 2912, 2932, 2945, 2967, 2989
$H\cdots trans\text{-}C_4H_8^{\ddagger}$	401 [199], 400 [264], 400 [384], 437, 472, 713, 822, 922, 956, 1017, 1018,1033, 1125, 1223, 1291, 1398, 1399, 1451, 1456, 1456, 1466, 1514, 2847, 2854, 2887, 2906, 2918, 2929, 2964, 2975
$H\cdots 1\text{-}C_4H_8^{\ddagger}$	283 [210], 331, 387, 417, 652, 759, 813, 900, 912, 956, 976, 1054, 1160, 1206, 1259, 1313, 1394, 1407, 1455, 1467, 1474, 1507, 2842, 2859, 2883, 2915, 2920, 2964, 2974, 3050
$sec\text{-}C_4H_9$[21]	2985, 2939, 2935, 2934, 2898, 2881, 2875, 2836, 2817, 1485, 1479, 1472, 1466, 1464, 1412, 1408, 1389, 1296, 1259, 1154, 1081, 1062, 991, 965, 954, 813, 753, 428, 401, 248
$cis\text{-}C_4H_8$[22]	3038, 2935, 2870, 1660, 1445 (3), 1406, 1260, 986, 870, 291, 2953, 1447, 1043, 871, 396, 2975, 1016, 675, 3023, 2949, 2876, 1462, 1383, 1135, 976, 570
$trans\text{-}C_4H_8$[22]	3009, 2973, 2869, 1682, 1444, 1385, 1306, 1142, 863, 500, 2950(2), 1442, 1043, 745, 1448, 1042, 963, 290, 3027, 2974, 2874, 1468, 1382, 1303, 1061, 978, 260
$1\text{-}C_4H_8$[23]	283, 331, 387, 417, 652, 759, 813, 900, 912, 956, 976, 1054, 1160, 1206, 1259, 1313, 1394, 1407, 1455, 1467, 1474, 1507, 2842, 2859, 2883, 2915, 2920, 2964, 2974, 3050
CH_3[24]	3184 (2), 3002, 1383(2), 580
C_3H_6[25]	3091, 3022, 2991, 2973, 2932, 1653, 1459, 1414, 1378, 1298, 1178, 935, 919, 428, 2953, 1443, 1045, 990, 912, 575

Moments of Inertia (amu $Å^2$), Symmetry Numbers, and Rotational Barriers (cm^{-1})

Overall Rotations

$CH_3\cdots CH_2CHCH_3^{\ddagger}$	$I_a = 38.9433$	$\sigma = 1$	(active)
	$(I_bI_c)^{1/2} = 144.513$	$\sigma = 1$	(inactive)
$H\cdots cis\text{-}C_4H_8^{\ddagger}$	$I_a = 36.3996$	$\sigma = 1$	(active)
	$(I_bI_c)^{1/2} = 114.637$	$\sigma = 1$	(inactive)
$H\cdots trans\text{-}C_4H_8^{\ddagger}$	$I_a = 19.3464$	$\sigma = 1$	(active)
	$(I_bI_c)^{1/2} = 143.553$	$\sigma = 1$	(inactive)
$H\cdots 1\text{-}C_4H_8^{\ddagger}$	$I_a = 23.8442$	$\sigma = 1$	(active)
	$(I_bI_c)^{1/2} = 134.956$	$\sigma = 1$	(inactive)
$sec\text{-}C_4H_9$[21]	$I_a = 18.963$	$\sigma = 1$	(active)
	$(I_bI_c)^{1/2} = 143.553$	$\sigma = 1$	(inactive)
$cis\text{-}C_4H_8$[22]	$I_a = 31.6993$	$\sigma = 1$	
	$(I_bI_c)^{1/2} = 109.77$	$\sigma = 2$	
$trans\text{-}C_4H_8$[22]	$I_a = 15.284$	$\sigma = 1$	
	$(I_bI_c)^{1/2} = 139.57$	$\sigma = 2$	
$1\text{-}C_4H_8$[26,27]	$I_a = 22.4111$	$\sigma = 1$	
	$(I_bI_c)^{1/2} = 123.119$	$\sigma = 1$	
CH_3[24]	$(I_aI_bI_c)^{1/3} = 2.21703$	$\sigma = 6$	
C_3H_6[25]	$(I_aI_bI_c)^{1/3} = 33.2762$	$\sigma = 1$	

Internal Rotations (line of Rotation Shown by "−")

$CH_3\cdots CH_2CHCH_3^{\ddagger}$	$I_r(CH_3\bullet\text{-}\bullet CH_2CHCH_3^{\ddagger}) = 3.1445$	$\sigma = 3$	$V_0 = 275.8$
	$I_r(CH_3\cdots CH_2CH{-}CH_3^{\ddagger}) = 2.9561$	$\sigma = 3$	$V_0 = 511.5$
$H\cdots cis\text{-}C_4H_8^{\ddagger}$	$I_r(CH_3CH_2CH{-}CH_3^{\ddagger}) = 2.9401$	$\sigma = 3$	$V_0 = 167.1$
	$I_r(CH_3{-}CH_2CHCH_3^{\ddagger}) = 2.93431$	$\sigma = 3$	$V_0 = 631.5$
$H\cdots trans\text{-}C_4H_8^{\ddagger}$	$I_r(CH_3CH_2CH{-}CH_3^{\ddagger}) = 2.65087$	$\sigma = 3$	$V_0 = 552.5$
	$I_r(CH_3{-}CH_2CHCH_3^{\ddagger}) = 2.65552$	$\sigma = 3$	$V_0 = 758.7$
$H\cdots 1\text{-}C_4H_8^{\ddagger}$	$I_r(CH_3{-}CH_2CHCH_3^{\ddagger}) = 2.81452$	$\sigma = 3$	$V_0 = 1240.4$
	$I_r(CH_3CH_2{-}CHCH_3^{\ddagger}) = 9.20605$	$\sigma = 1$	$V_0 = 693$ (3 minima)
$sec\text{-}C_4H_9$[21]	$I_r(CH_3{-}CH_2CHCH_3) = 3.0309$	$\sigma = 3$	$V_0 = 1151$
	$I_r(CH_3CH_2CH{-}CH_3) = 3.0321$	$\sigma = 3$	$V_0 = 178$
	$I_r(CH_3CH_2{-}CHCH_3) = 9.68198$	$\sigma = 1$	$V_0 = 755$
$cis\text{-}C_4H_8$:[22,28]	$I_{r,1,2}(CH_3{-}CHCHCH_3) = 3.127$	$\sigma = 3$	$V_0 = 250$
$trans\text{-}C_4H_8$:[22,29]	$I_{r,1,2}(CH_3{-}CHCHCH_3) = 2.63912$	$\sigma = 3$	$V_0 = 861$
$1\text{-}C_4H_8$:[26,27]	$I_r(CH_3{-}CH_2CHCH_2) = 2.8821$	$\sigma = 3$	$V_0 = 1104$
	$I_r(CH_3CH_2{-}CHCH_2) = 7.6834$	$\sigma = 1$	$V_0 = 666$ (3 minima)
C_3H_6:[25]	$I_r(CH_3{-}CH_2CH_2) = 2.3765$	$\sigma = 3$	$V_0 = 700$

Numbers of Optical Isomers, *m*, (if More Than One)

$m(CH_3\cdots CH_2CHCH_3^{\ddagger}) = 2$	$m(H\cdots cis\text{-}C_4H_8^{\ddagger}) = 2$	$m(H\cdots trans\text{-}C_4H_8^{\ddagger}) = 2$	$m(H\cdots 1\text{-}C_4H_8^{\ddagger}) = 2$

Lennard-Jones Parameters

molecule	$sec\text{-}C_4H_9$	$cis\text{-}C_4H_8$	He	Ar	Kr	Ne	N_2
σ/Å	4.687	4.687	2.551	3.542	3.655	2.820	3.798
ϵ/K	531.4	531.4	10.22	93.3	178.9	32.8	71.4
ref	*a*	*a*	30	30	30	30	30
molecule	H_2 (D_2)	CO_2	CH_4	SF_6	CD_3F	CH_3Cl	
σ/Å	2.827	3.941	3.758	5.128	3.981	4.182	
ϵ/K	59.7	195.2	148.6	222.1	235.7	350	
ref	30	30	30	30	*b*	30	

TABLE 1 (Continued)

Reaction Barriers (kJ mol^{-1}), Tunneling Barrier "Width" (l, amu$^{1/2}$ Å), and Corresponding Imaginary Frequencies (cm^{-1}):			
$E^0_{1ac} = 9.7$	$E^0_{1at} = 9.9$	$E^0_{1a\alpha} = 7.3$	$E^0_{1b} = 32.3$
$E^0_{-1ac} = 152.8$	$E^0_{-1at} = 148.4$	$E^0_{-1a\alpha} = 157.8$	$E^0_{-1b} = 129.7$
$l_{1ac} = 1.83$	$l_{1at} = 1.78$	$l_{1a\alpha} = 1.83$	
$\nu^i_{1ac} = 642$	$\nu^i_{1at} = 662$	$\nu^i_{1a\alpha} = 574$	
Experimental High-Pressure-Limit Rate Expressions Used in Determination of Transition State Properties (cm^3 molecule^{-1} s^{-1}):			
$k^\infty_{-1ac} = 2.89 \times 10^{-11}$ exp(−1083 K/T)[16]	$k^\infty_{-1at} = 3.46 \times 10^{-11}$ exp(−1043 K/T)[16]	$k^\infty_{-1a\alpha} = 3.77 \times 10^{-11}$ exp(−942 K/T)[16]	$k^\infty_{-1b} = 1.81 \times 10^{-12}$ exp(−4239 K/T)[c]

[a] Taken as equal to that of *n*-C_4H_{10}.[30] [b] Calculated from boiling point and additive volume increments.[30] [c] References 12, 31−33; see text.

6-31G(d,p) levels. Values of torsional barriers obtained at UHF and UMP2 levels agree within 2.5 kJ mol^{-1}. UMP2 values were used in the model. Detailed results of ab initio calculations of transition states are presented in the Supplement. The GAUSSIAN 94 system of programs[43,44] was used in all ab initio calculations. The results of ab initio calculations on the lowest-energy conformation of the transition state for reaction 1b nearly coincide with those reported by Gang et al.[45] These authors, however, did not obtain data for conformations with methyl groups turned, which warranted our own present study of this transition state.

Tunneling can be expected to play a significant role in reactions 1ac, 1at, and 1aα since each involves a transfer of an H atom. The treatment of tunneling in the current work follows the approach used by Knyazev and Slagle[46] and Knyazev et al.[47] in their modeling of the $C_2H_3 \leftrightarrow H + C_2H_2$ and $C_2H_3 + H_2 \leftrightarrow H + C_2H_4$ reactions. Computation of under-barrier tunneling and above-barrier reflection probabilities is based on the knowledge of the barrier "width". To determine the "width" parameters of these reactions, the shapes of the barriers of reactions 1c and 1t were determined using the method of reaction path following (intrinsic reaction coordinate, IRC)[48,49] in mass-weighted internal coordinates.[49] For each point on the reaction path, optimization was done at the UHF/6-31G(d) level and energy was computed at the UMP2/6-31G(d,p) level. The potential energy profile along the reaction path was fitted with the Eckart function

$$V = \frac{A\xi}{(1+\xi)} + \frac{B\xi}{(1+\xi)^2} \qquad \xi = \exp\left(\frac{2\pi x}{l}\right) \qquad \text{(II)}$$

where x is a coordinate along the reaction path, l is the "width" parameter, and parameters A and B are related to the barriers for the direct and reverse reactions E_1 and E_{-1}:

$$A = \Delta E_{1,-1} = E_1 - E_{-1} \qquad B = (\sqrt{E_1} + \sqrt{E_{-1}})^2 \qquad \text{(III)}$$

The transition probability for such a barrier can be described analytically, as shown by Eckart.[50] In the fitting process, parameter A was fixed at the value obtained from ab initio calculations, and B and l were determined from the fitting. Only points with energy above that of $H + C_4H_8$ were used. Potential energy profiles obtained in the calculations and details of the calculations are presented in the Supplement. The values of the "width" parameter l obtained in UHF and MP2 level calculations are close to each other for both reactions 1ac and 1at (l(1ac) = 2.22 (UHF) or 1.83 (UMP2) amu$^{1/2}$ Å; l(1at) = 2.12 (UHF) or 1.78 (UMP2) amu$^{1/2}$ Å). The authors of refs 46 and 47 found that further improvement of the level of ab initio theory (to UMP4 and spin-projected PMP4[51] methods) did not results in significant changes of the "width" parameter l for the $C_2H_3 \leftrightarrow H + C_2H_2$ and $C_2H_3 + H_2 \leftrightarrow H + C_2H_4$ reactions. This is not surprising since l is, essentially, a geometrical parameter, and, as such, can be expected to be determined with good accuracy even by relatively low-level ab initio methods. Thus, UMP2 values of l were used in the model for reactions 1ac and 1at. Since the values of l for reactions 1ac and 1at are close, one can expect that the l parameter for reaction 1aα will have a similar value. Thus, no IRC calculations were performed for reaction 1aα and the width parameter l(1aα) = 1.83 amu$^{1/2}$ Å was taken to be equal to that of reaction 1ac.

High-pressure-limit rate constants were computed using the transition state theory formula[52]

$$k^\infty_{A+B}(T) = \frac{k_B T \kappa(T) Q^{\ddagger}}{h \; Q_A Q_B} \exp\left(-\frac{E_0}{k_B T}\right) \qquad \text{(IV)}$$

where $Q^{\ddagger}$, Q_A, and Q_B are partition functions of the transition state and reactants A and B, respectively, E_0 is the reaction energy barrier, and $\kappa(T)$ is the temperature-dependent tunneling factor:

$$\kappa(T) = \int_{-E_0}^{\infty} P'(E) \exp\left(-\frac{E}{k_B T}\right) dE \qquad \text{(V)}$$

Here, $P'(E)$ is the first derivative of the energy-dependent tunneling transition probability $P(E)$, which was calculated using the analytical formula of Eckart.[50]

II.3. Solution of the Master Equation and Modeling of Pressure-Dependent Rate Constants and Channel Branching Fractions. *Solution of the Master Equation.* Modeling of both the chemically activated and the thermally activated decomposition reaction of secondary butyl radical requires a solution of the corresponding master equation[2] that explicitly describes the interplay of energy-dependent reactions, activation, and collisional energy transfer. For the chemically activated reaction corresponding to the conditions of the experiments of Rabinovitch and co-workers, the temporal evolution of the energy- and time-dependent population of *sec*-C_4H_9 $g(E,t)$ is determined by the following form of the master equation:

$$\frac{\partial g(E,t)}{\partial t} = \omega \int_0^{\infty} [P(E,E')\, g(E',t) - P(E',E)\, g(E,t)]\, dE' - k(E)\, g(E,t) + x(E) k^\infty_{-1an} [H][C_4H_8] \qquad \text{(VI)}$$

Here, ω is the frequency of collisions with the bath gas, $P(E,E')$ is the probability of energy transfer upon collision (from energy level E' to energy level E), $k(E)$ is the overall energy-dependent reaction rate constant for decomposition via all possible channels,

$$k(E) = k_{1b}(E) + k_{1at}(E) + k_{1ac}(E) + k_{1a\alpha}(E) \qquad \text{(VII)}$$

$x(E)$ is the chemical activation distribution function, [H] and [C_4H_8] are the concentrations of H and butene, respectively, and k^∞_{-1an} (n = t, c, or α) is the high-pressure-limit rate constant of the addition of H atom to butene, the activating

reaction. The functional form of $x(E)$ has been derived from detailed balance considerations by Rabinovitch and Diesen[4] and can be expressed as[2,14]

$$x(E) = \frac{k_{1an}(E)\, f(E)}{k_{1an}^{\infty}} \qquad \text{(VIII)}$$

where $f(E)$ is the normalized Boltzmann distribution of *sec*-C_4H_9.

By dividing the energy axis into an array of small energy "bins" of the size δE and replacing continuous functions with vectors, one can represent eq VI in a matrix form (see, for example, ref 2):

$$\frac{d\mathbf{g}(t)}{dt} = \mathbf{J}\mathbf{g}(t) + \mathbf{x}(t)k_{-1an}^{\infty}[H][C_4H_8] \qquad \text{(IX)}$$

where

$$J_{i,l} = \begin{cases} \omega P(E_i,E_l)\ \delta E & i \neq l \\ -k(E) - \delta E \omega \sum_{l \neq i} P(E_l,E_i), & i = l \end{cases}$$

The general behavior of the solution of master equation of the type given by eqs VI and IX under the assumption of weak collisions[2] has been described by Schranz and Nordholm[53] and later by Smith et al.[54]

The case of the thermally activated decomposition of secondary butyl radical is described by the same master equation VI (or IX) but with the last term ($x(E)k_{-1an}^{\infty}[H][C_4H_8]$) removed. The conditions of the experiments of Rabinovitch and co-workers[4-11] and of Knyazev et al.[12] correspond to the steady-state regime[2,53,54] where the shape of the energy distribution of reacting *sec*-C_4H_9 molecules (in the case of the chemically activated system, the shape of the distribution above the lowest barrier) does not change with time. In the case of the thermally activated reaction, the steady-state decomposition rate constant ($k_2(T,[M])$) is equal to the lowest (in absolute value) eigenvalue of the matrix **J** of the master equation IX (see, for example, ref 2 for a detailed discussion of the solution, its interpretation, and properties of thermally activated unimolecular reactions). Solution of the master equation for the chemically activated system requires a more detailed description which is presented below.

To solve the master equation VI (IX) and express the results in terms of rate constants, the *virtual components* formalism of Knyazev and Tsang[13] was applied. This formalism has been developed to enable the interpretation of the general case of unimolecular kinetics (including non-steady-state behavior,[13,53,55-59] when the rates of reactions change in time together with the rapidly evolving energy distributions) in terms of time-independent rate constants. Such interpretation enables incorporation of non-steady-state kinetics into large reaction schemes, such as those used to model the chemistry of combustion. The *virtual components* formalism provides, as a limiting, specific case of the general solution, the steady-state rate constants of chemically or photochemically activated unimolecular reactions.

The method is based on representing the overall population of the active molecule (*sec*-C_4H_9) as a combination of "virtual components" due to eigenvectors of the master equation matrix. In the steady-state case, the spectrum of characteristic rates of evolution of virtual components (given by the absolute values of the corresponding eigenvalues $|\lambda_j|$ of **J**) contains one value that is significantly (by orders of magnitude) lower than the rest of the rates.[2,13,53,54] This virtual component with the lowest rate of evolution (decay or decomposition) is associated with the stabilized molecules. The energy distribution of stabilized molecules is that of this "first" virtual component. Because of the very fast evolution of the rest of the virtual components, their kinetics do not need to be considered explicitly and their contribution can be described jointly as pseudo-bimolecular reaction(s) leading directly from reactants to products of decomposition as if "bypassing" the active intermediate.

The chemically activated reaction of (1) can thus be represented by the following combination of reactions:

$$H + C_4H_8 \rightarrow \textit{sec}\text{-}C_4H_9 \qquad \text{(S)}$$

$$H + C_4H_8 \rightarrow CH_3 + C_3H_6 \qquad \text{(D)}$$

$$\textit{sec}\text{-}C_4H_9 \rightarrow CH_3 + C_3H_6 \qquad (2)$$

Reactions S, D, and 2 can be described as "pseudo-reactions" in a sense that they do not exactly represent elementary processes but rather, taken together, present a simple way of accurately describing a more complex process. Reaction S describes the formation of *stabilized* (or *thermalized)* secondary butyl radicals, reaction 2 describes the thermal (or thermally activated) decomposition of stabilized radicals, and reaction D accounts for the formation and immediate decomposition of those vibrationally excited (chemically activated) *sec*-butyl radicals that were not stabilized by collisions with the bath gas. In terms of the *virtual components* formalism, reaction S is the formation of the first virtual component and reaction 2 is the thermal decomposition of the first virtual component. Reaction D is the pseudo-direct reaction leading from reactants to products (as if bypassing the active molecule, *sec*-C_4H_9) that appears due to joint contribution of all virtual components except for the first one. Here, the reaction numbering is purposefully different from that used in (1) in order to distinguish between elementary energy-dependent processes appearing in (1), on one hand, and reactions of thermalized species (S, 2, D), which are the results of interpretation through the *virtual components* formalism, on the other. The exact isomer of butene is not specified in reactions S and D since it can be any of the three isomers that produce *sec*-C_4H_9 as a result of addition of H atom. In fact, all three isomers (cis, trans, and 1-butene) were used in the experiments of Rabinovitch and co-workers.

Reactions S, 2, and D are the most important processes occurring in the chemically activated system. However, if a complete description is desired, channels involving decomposition of secondary butyl radical to H atoms and isomers of butene must be included. The complete reaction scheme, thus, also includes the reactions

$$\textit{sec}\text{-}C_4H_9 \rightarrow H + \textit{cis}\text{-}C_4H_8 \qquad (2')$$

$$\textit{sec}\text{-}C_4H_9 \rightarrow H + \textit{trans}\text{-}C_4H_8 \qquad (2'')$$

$$\textit{sec}\text{-}C_4H_9 \rightarrow H + 1\text{-}C_4H_8 \qquad (2''')$$

$$H + C_4H_8 \rightarrow H + \textit{cis}\text{-}C_4H_8 \qquad (D')$$

$$H + C_4H_8 \rightarrow H + \text{trans} - C_4H_8 \qquad (D'')$$

$$H + C_4H_8 \rightarrow H + 1\text{-}C_4H_8 \qquad (D''')$$

Of course, one of the "D" reactions (D′, D″, or D‴) is the reverse of the $H + C_4H_8$ activating reaction, depending on the particular isomer of butene used. All of the above channels were included in the model. However, as the results of calculations indicated, the contributions of channels 2′, 2″, 2‴, D′, D″, and

D‴ are negligible (less than 1% of reactions 2 and D, respectively) under the experimental conditions of Rabinovitch and co-workers and Knyazev et al.

The rate constants of reactions S, 2, and D, within the formalism of *virtual components*, are given by the following equations:[13]

$$k_S = k_{1an}^{\infty}\Phi_1\sum_i \frac{e_1(E_i)}{f(E_i)}x(E_i)\,\delta E \qquad (X)$$

$$k_2 = {\Phi_1}^{-1}\sum_i k_{1b}(E_i)\,e_1(E_i)\,\delta E \qquad (XI)$$

$$k_D = k_{1an}^{\infty}\sum_i \frac{x(E_i)}{f(E_i)}b_{1b}(E_i)\,\delta E \qquad (XII)$$

where $b_{1b}(E)$ is a *correlation function*[13] for channel 1b

$$b_{1b}(E) = \sum_{j\geq 2} e_j(E)|\lambda_j|^{-1}\sum_i k_{1b}(E_i)\,e_j(E_i)\,\delta E \qquad (XIII)$$

Here, $e_j(E)$ is a jth eigenvector of matrix **J** corresponding to an eigenvalue λ_j, index i numbers energy levels, and $\Phi_j = \sum_i e_j(E_i)\,\delta E$. Eigenvectors and eigenvalues of **J** are numbered in the same way as *virtual components*; i.e., the "first" eigenvalue is the lowest one in absolute value.

Eigenvalues and eigenvectors of matrix **J** were obtained via the method based on Householder's tridiagonalization algorithm[60] which was used earlier by Bedanov et al.[61] and Tsang et al.[58] Calculations were performed using the computer program *ChemRate*[62] with 50 cm^{-1} energy bin size. A 10 times smaller (5 cm^{-1}) energy bin size was used to compute sums and densities of states and energy dependent microscopic reaction rate constants ($k(E)$). Sums and densities of states of secondary butyl radical and transition states were calculated using the modified Beyer−Swinehart algorithm.[63] Contributions of hindered rotors were included via the method of Knyazev.[64] Reduced moments of inertia of internal hindered rotors were calculated via the method of Pitzer and Gwinn.[65] It has been demonstrated[64] that rotational densities of states thus computed provide an excellent approximation to those obtained via exact treatment[45,66] of external-internal rotational coupling. Microscopic energy-dependent rate constants $k(E)$ were computed using the RRKM method.[1−3] Tunneling was included in $k(E)$ RRKM calculations via the method developed by Miller[67] and, at the same time, by Kato and Morokuma.[68] Energy dependent tunneling probabilities $P(E)$ were obtained using the Eckart[50] formula, as described in subsection II.2. Reaction path degeneracies were calculated from rotational symmetry numbers and numbers of optical isomers (Table 1) using the formula of Gilbert and co-workers.[2,69] Conservation of angular momentum was approximately taken into account by multiplying the $k(E)$ values obtained in RRKM calculations by the factor $I^{\neq}/I$, where $I^{\neq}$ and I are the moments of inertia of the 2-dimensional adiabatic[1−3] rotational degrees of freedom of the transition state and active molecule, respectively. Such correction of microscopic rates ensures that the high-pressure-limit rate constants of individual reaction channels computed by averaging of microscopic rates over the Boltzmann distribution coincide with those calculated via the transition state theory formula. Although this correction of $k(E)$ by the $I^{\neq}/I$ factor does not provide an exact description of the angular momentum conservation effects in the falloff, the inaccuracies thus introduced are expected to be minor since the values of the two-dimensional inactive (adiabatic) moments of inertia of the transition states involved in the reactive system are close to those of the active molecule, *sec*-C_4H_9 (Table 1). In particular, the $I^{\neq}/I$ factor for the most important transition state, that for the decomposition to $CH_3 + C_3H_6$, differs from 1 by less than one percent.

The exponential-down[2,70] model of collisional energy transfer

$$P(E,E') = C\exp\left(-\frac{E'-E}{\alpha(T,E')}\right) \qquad E < E' \qquad (XIV)$$

was used. The probability of "downward" collisional energy transfer is given by expression XIV and that of "upward" transfer is obtained from detailed balance (see, for example, ref 2). Here, C is a normalization constant and the parameter $\alpha(T,E')$ coincides with $\langle\Delta E\rangle_{down}$, the average energy transferred per "downward" collision,[2] at all energies $E' \gg \alpha(T,E')$. In general, the $\langle\Delta E\rangle_{down}$ parameter is both temperature and energy dependent. The temperature dependence will be discussed further below. The energy dependence of $\langle\Delta E\rangle_{down}$ is a subject of current research (see, for example, refs 71−75 for reviews of literature). The existence of this dependence is, however, well established. Effects of such energy dependence on calculated thermal reaction rates are nonnegligible.[76] Generally, $\langle\Delta E\rangle_{down}$ increases with energy, the functional form of this increase being dependent on the particular system of excited molecule and bath gas collider. In the absence of exact knowledge of the functional form for the secondary butyl radical, we use an approximation to account for the $\langle\Delta E\rangle_{down}$ vs energy dependence. In this approximation, $\alpha(T,E')$ increases linearly with energy, changing by a factor of 2 in the energy range $0-E_{1b}^0$ (E_{1b}^0 is the barrier for channel 1b):

$$\alpha(T,E') = \frac{1}{2}\alpha_0(T,E')\left[1 + \frac{E'}{E_{1b}^0}\right] \qquad (XV)$$

Thus, $\alpha(T,E') = {}^1/_2\alpha_0(T,E')$ at $E' = 0$ and $\alpha(T,E') = \alpha_0(T,E')$ at $E' = E_{1b}^0$. This α vs E' dependence is in approximate agreement with the recommendations of Hold et al.,[74] which were based on these authors' experimental study of collisional deactivation of highly vibrationally excited toluene and azulene. The term $\langle\Delta E\rangle_{down}$ will be used henceforth to designate $\alpha_0(T,E')$.

Modeling of Pressure-Dependent Rate Constants and Channel Branching Fractions. First Approximation. The thermodynamic data on the chemical species involved in the chemical system described by eq 1 (subsection II.1) and the properties of all the transition states obtained from ab initio calculations and adjusted to reproduce experimental data on the high-pressure rates of addition reactions (subsection II.2) determine all the features of the model required to calculate the rate constants and branching fractions with the exception of $\langle\Delta E\rangle_{down}$, the average energy transferred per deactivating collision. However, all experimental data upon which the model is built are determined with a finite degree of accuracy and thus have nonzero uncertainty limits. The most uncertain parameter in the model is the standard enthalpy of formation of secondary butyl radical. The value used in the model construction, $\Delta_f H°_{298}$(*sec*-C_4H_9) = 67.5 kJ mol^{-1},[37] has a reported uncertainty of ±2.3 kJ mol^{-1}. While it is desirable to investigate the influence of variations in all parameters on the results of modeling, the large number of reaction channels and transition states involved in the reaction system under study makes such comprehensive uncertainty evaluation impractical. However, the influence of the $\Delta_f H°_{298}$(*sec*-C_4H_9) value on the modeling results is quite substantial and will be a subject of separate discussion later in this subsection. First, the results of modeling experimental data using

the "first approximation" model (i.e., the model with $\Delta_f H°_{298}$(*sec*-C_4H_9) = 67.5 kJ mol^{-1}, as reported in ref 37) will be reported. Second, the influence of small variations of $\Delta_f H°_{298}$(*sec*-C_4H_9) on the results will be discussed and a "final" adjusted version of the model will be presented. More on model uncertainties is presented in Discussion, section III.

The "first approximation" model was used to reproduce the experimental values of $S/(S + D)$ ratios (i.e., branching fractions of formation of stabilized *sec*-butyl radicals) in the chemical activation experiments of Rabinovitch and co-workers, as well as experimentally obtained thermal rate constants reported by Knyazev et al.[12] Most data in both the chemically activated and thermally activated experimental systems were obtained in helium bath gas. Therefore, in our modeling effort, attention was focused on reproducing experimental results obtained in helium.

In all experiments of Rabinovitch and co-workers, noticeable fractions of butene (in the majority of experiments, *cis*-C_4H_8, 2.1−10%) were present in the bath gas. Since butene is, most likely, a stronger collider than most of the other bath gases used, one needs to account for its influence on the branching fractions. For this purpose, $\langle\Delta E\rangle_{down}(C_4H_8)$ values must be obtained. Thus, the first modeling attempt was directed at reproducing stabilization branching fractions ($S/(S + D)$ ratios) obtained using pure *cis*-C_4H_8 as bath gas in the experiments on the chemically activated decomposition of *sec*-butyl in the reaction of H atoms with *cis*-butene by Diesen and Rabinovitch[4] and Kohlmaier and Rabinovitch.[9,10] At each experimental temperature (170, 195, 298, and 373 K), $\langle\Delta E\rangle_{down}$(*cis*-$C_4H_8$) was adjusted to achieve the best agreement between the calculated and experimental values of the $S/(S + D)$ ratio. The sum of squares of deviations was minimized to achieve the best fit. Each data point was assigned a weight equal to the reciprocal of $S/(S + D)$. Such weighting represents an intermediate case between an unweighted fit (which would give unfairly large weights to high-pressure-end results) and fitting "on a logarithmic scale" (minimizing the sum of squares of deviations of logarithms), which would treat relative deviations at low and high pressures equally. Considering the fact that low-pressure-end data are less reliable due to the "low-pressure artifact" (see subsection II.1), we choose the reciprocal weighting method of data fitting, which gives some preference to higher pressure data but takes low-pressure results into account as well.

The results of fitting the data obtained in *cis*-C_4H_8 as bath gas are presented in Figure 1. The main plot shows the experimental $S/(S + D)$ values (symbols) and calculated curves (lines) while the inset (hollow circles) presents the temperature dependence of the fitted values of $\langle\Delta E\rangle_{down}$. $\langle\Delta E\rangle_{down}$ obtained in the fitting displays a strong positive temperature dependence with values changing from 142 cm^{-1} at 170 K to 515 cm^{-1} at 373 K (Table 2).

These $\langle\Delta E\rangle_{down}$ values were then used in modeling the experiments performed with helium as bath gas. Since minor but noticeable fractions of butene were present in helium, the overall collisional energy transfer probability function $P_{all}(E,E')$ was constructed from the corresponding functions of individual colliders:

$$\omega_{all}P_{all}(E,E') = \omega_{He}P_{He}(E,E') + \omega_{C_4H_8}P_{C_4H_8}(E,E') \quad \text{(XVI)}$$

Here, ω_{all}, ω_{He}, and $\omega_{C_4H_8}$ are collision frequencies with all bath gas molecules, with helium, and with butene, respectively. Fitting results are presented in Figures 2 and 3: calculated vs experimental pressure dependencies curves (Figure 2) and $\langle\Delta E\rangle_{down}$(He) as a function of temperature (Figure 3, hollow circles). The three calculated lines obtained at room temperature for experimental conditions with different content of butene in bath gas (10%, 5.9%, and 2.1%) demonstrate nonnegligible differences between them.

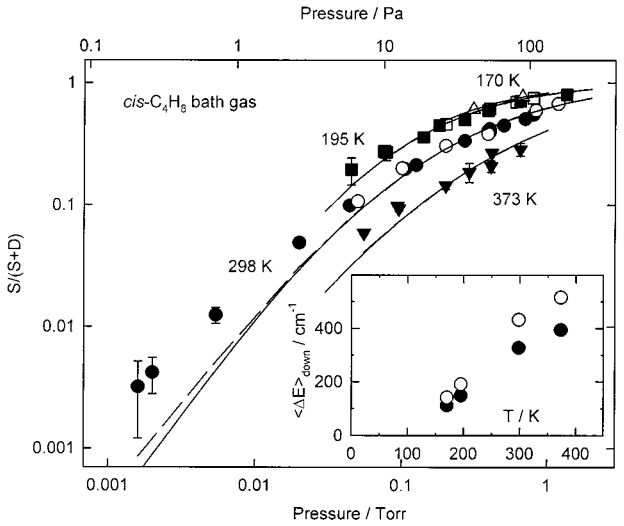

Figure 1. Main plot: experimental (symbols) and calculated (lines) pressure dependencies (falloffs) of stabilization branching fractions in the reaction of H atoms with *cis*-C_4H_8 in *cis*-C_4H_8 bath gas. Experimental data are from Rabinovitch and Diesen[4] (open symbols) and Kohlmaier and Rabinovitch[9,10] (filled symbols). Calculated curves are obtained with the first approximation (dashed lines) and the final models (solid lines; see subsection II.3). Differences between the lines obtained using the first approximation and the final model are negligible at pressures above 2.7 Pa (0.02 Torr). Symbols: triangles up (170 K), squares (195 K), circles (298 K), and triangles down (373 K). Experimental uncertainties shown are estimated in the current work from corrections for "low-pressure artifact";[4,9,10] see text (subsection III.1). Inset: temperature dependencies of $\langle\Delta E\rangle_{down}$(*cis*-$C_4H_8$) obtained in modeling the experimental falloffs with the first approximation model (open symbols) and final model (filled symbols).

TABLE 2: Values of $\langle\Delta E\rangle_{down}$ Obtained in Fitting Experimental Chemical Activation Data (cm^{-1})

	temperature/K			
bath gas	170	195	298	373
First Approximation Model				
cis-C_4H_8	142	191	432	515
He		127	196	236
Final Model				
cis-C_4H_8	112	149	327	394
He	-	102	158	192
Ar	-	102	174	230
Kr	-	95	194	219
Ne	-	115	178	204
N_2	-	112	217	222
H_2	-	84	143	169
D_2	-	77	153	198
CO_2	-	-	239	-
CH_4	-	-	269	-
SF_6	-	-	301	-
CD_3F	-	-	327	-
CH_3Cl	-	-	273	-

The $\langle\Delta E\rangle_{down}$(He) vs temperature dependence shown by the open circles in Figure 3 is best represented with a directly proportional dependence $\langle\Delta E\rangle_{down}(He) = 0.643T$ cm^{-1} (T expressed in K). Such proportional dependence is not surprising. A similar dependence, $\langle\Delta E\rangle_{down}(He) = 0.255T$ cm^{-1}, was obtained[76,77] in a study of the reaction

$$C_2H_5 \leftrightarrow H + C_2H_4 \quad (3,-3)$$

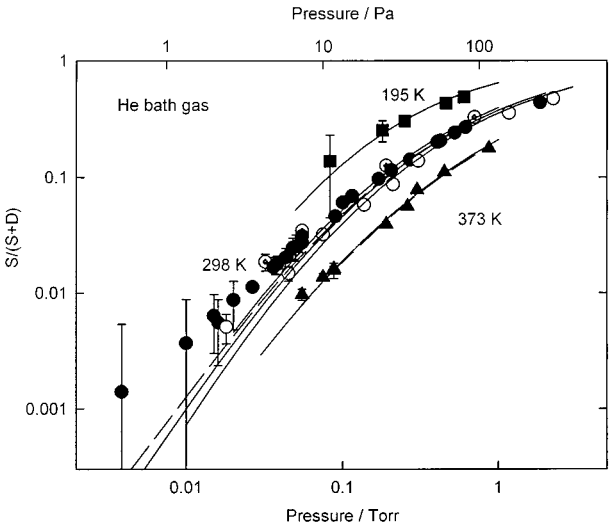

Figure 2. Experimental (symbols) and calculated (lines) pressure dependencies (falloffs) of stabilization branching fractions in the reaction of H atoms with *cis*-C_4H_8 in He bath gas (with a small fraction of *cis*-C_4H_8). Experimental data are from Kohlmaier and Rabinovitch.[9,10] Calculated curves are obtained with the first approximation (dashed lines) and the final models (solid lines; see subsection II.3). Symbols: squares (195 K), circles (298 K), and triangles (373 K). Three types of circles and three solid lines at 298 K correspond to three different fractions of *cis*-C_4H_8 in the bath gas: 2.1% (open circles), 5.9% (filled circles), and 10% (crossed open circles). Only one line calculated using the first approximation model (obtained with 5.9% of butene) is shown at 298 K to avoid plot congestion. Differences between the lines obtained using the first approximation and the final model are negligible at 195 and 373 K Experimental uncertainties shown are estimated in the current work from corrections for "low-pressure artifact";[4,9,10] see text (subsection III.1).

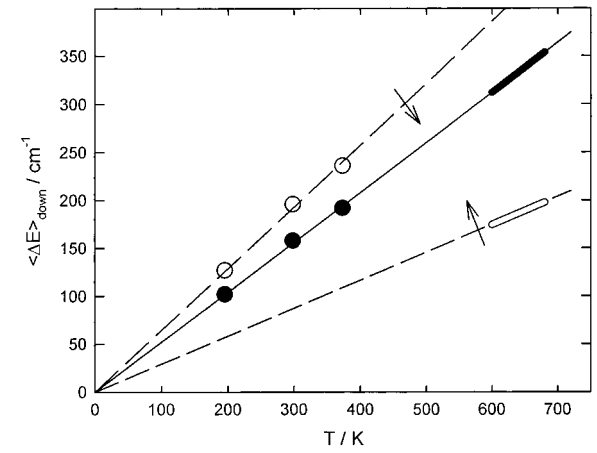

Figure 3. $\langle\Delta E\rangle_{down}$(He) vs temperature dependencies obtained in fitting experimental falloff data. Symbols: $\langle\Delta E\rangle_{down}$(He) values obtained from fitting data[9,10] on chemically activated reaction. Wide lines: results of modeling of the data[12] on thermal decomposition of *sec*-C_4H_9 radical. Open symbols and hollow wide line are obtained with the first approximation model, filled symbols and filled wide line with the final model. Thin lines: linear proportional fits (dashed lines, first approximation model; solid line, final model). Arrows indicate the directions of change resulting from lowering the heat of formation of *sec*-C_4H_9.

where experimental data on falloff in both direct and reverse reactions were reproduced by weak collision RRKM/master equation modeling at temperatures ranging from 298 to 1100 K. Modeling of two other radical decomposition reactions (*i*-$C_3H_7 \leftrightarrow H + C_3H_6$,[78] $C_2H_3 \leftrightarrow H + C_2H_2$[46]) indicated a preference for a positive temperature dependence of $\langle\Delta E\rangle_{down}$, although the functional forms of these dependencies used in modeling were different from direct proportionality. A more detailed discussion of the temperature dependence of $\langle\Delta E\rangle_{down}$ is presented in the Discussion (section III).

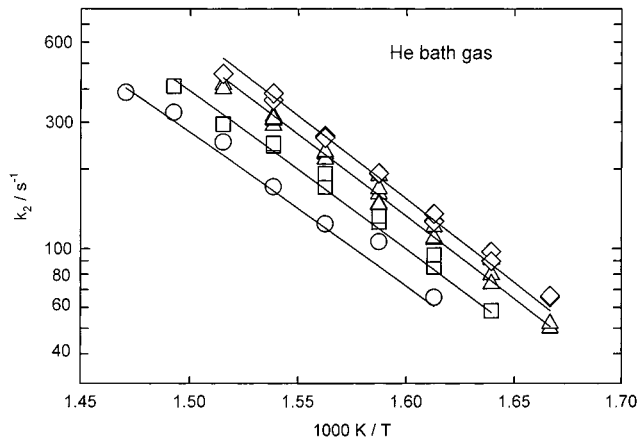

Figure 4. Experimental (symbols) and calculated (lines) rate constants of thermal decomposition of *sec*-C_4H_9 in He bath gas. Experimental data are from Knyazev et al.[12] Calculated lines are obtained by master equation modeling (current work, final model). Circles, [He] = 3×10^{16} molecules cm^{-3}; squares, [He] = 6×10^{16} molecules cm^{-3}; triangles, [He] = 12×10^{16} molecules cm^{-3}; diamonds, [He] = 18×10^{16} molecules cm^{-3}.

Fitting of the thermal decomposition data in helium as bath gas was performed in an analogous manner, by minimizing the sum of squares of deviations between experimental and calculated first-order rate constants. Each data point was assigned a weight equal to the reciprocal of the experimental rate constant value. In fitting the thermal decomposition data, the proportional $\langle\Delta E\rangle_{down}$ vs temperature dependence was imposed and the proportionality coefficient was used as an adjustable parameter. This functional form of the $\langle\Delta E\rangle_{down}$ vs T dependence was selected on the basis of the results of modeling of the chemical activation data, see above. The results of the fitting (calculated vs experimental rate constants and the obtained $\langle\Delta E\rangle_{down}$ vs T dependence, $\langle\Delta E\rangle_{down}(He) = 0.291T$ cm^{-1}) are displayed in Figures 4 and 3 (wide hollow line).

Modeling of Pressure-Dependent Rate Constants and Channel Branching Fractions. Final (Adjusted) Model. As can be seen from Figure 3, the $\langle\Delta E\rangle_{down}$ vs T dependencies obtained from fitting experimental data on chemical and thermal activation diverge (hollow circles and wide hollow line). Both display proportional dependencies (resulting from data fitting in the chemical activation case and imposed artificially in the thermal activation case) but the proportionality coefficients differ by a factor of 2.2. However, it was observed that these proportionality coefficients display a strong dependence on the value of the secondary butyl radical heat of formation. Furthermore, the effects of variation of the value of the *sec*-C_4H_9 heat of formation have opposite signs for chemical and thermal activation data sets. For example, increasing $\Delta_fH°_{298}$(*sec*-C_4H_9) (thus reducing the *sec*-butyl potential well depth and the barrier to decomposition to $CH_3 + C_3H_6$) has the effect of increasing the thermal decomposition rates, $k_2(T,[M])$, but decreasing the efficiency of stabilization in the chemical activation case. This, in turn, would result in lower fitted values of $\langle\Delta E\rangle_{down}$ in the thermal decomposition case and in higher $\langle\Delta E\rangle_{down}$ obtained from the chemical activation data. A decrease in $\Delta_fH°_{298}$(*sec*-C_4H_9) would have an opposite effect. The directions of change in the fitted $\langle\Delta E\rangle_{down}$ vs T dependencies due to $\Delta_fH°_{298}$(*sec*-C_4H_9) variation are indicated in Figure 3 by arrows. The sensitivity of the fitted $\langle\Delta E\rangle_{down}$ values to $\Delta_fH°_{298}$(*sec*-C_4H_9) is

such that a relatively minor change of $\Delta_f H°_{298}(sec\text{-}C_4H_9)$ by -3.4 kJ mol^{-1} results in an agreement between the $\langle\Delta E\rangle_{down}$ vs T linear dependencies obtained from fitting the chemical activation data, on one hand, and thermal activation data, on the other. Filled symbols and the wide solid line in Figure 3 indicate the $\langle\Delta E\rangle_{down}$ vs T dependence obtained with the thus modified model. This dependence can be best represented with the expression (shown by the thin solid line in Figure 3)

$$\langle\Delta E\rangle_{down}(He) = 0.520T \text{ cm}^{-1} \qquad (T \text{ expressed in K}) \tag{XVII}$$

Pressure dependencies of $k_2(T,[M])$ and $S/(S + D)$ calculated using the adjusted model and formula XVII are demonstrated in Figures 2 and 4. The adjusted value of $\Delta_f H°_{298}(sec\text{-}C_4H_9) = 64.1$ kJ mol^{-1} is adopted for further use in the final optimized version of the model. Figure 1 shows the results of fitting the chemical activation data obtained in *cis*-butene bath gas with the final model.

The difference of 3.4 kJ mol^{-1} between the adjusted value of $\Delta_f H°_{298}(sec\text{-}C_4H_9) = 64.1$ kJ mol^{-1} and the experimental value of Seakins et al.[37] (67.5 kJ mol^{-1}), although being comparable with the reported[37] uncertainty of the experimental value (± 2.3 kJ mol^{-1}), still exceeds the latter. The reported uncertainty of Seakins et al. originates, mainly, not in experimental measurements but in the estimated uncertainties in the calculated entropy of the *sec*-butyl radical. The addition of the uncertainty (± 0.7 kJ mol^{-1})[79] in the heat of formation of *n*-C_4H_{10} (used by the authors of ref 37) increases the uncertainty of $\Delta_f H°_{298}(sec\text{-}C_4H_9)$ to 3.0 kJ mol^{-1}. This serves to demonstrate that the amount of adjustment in the *sec*-butyl radical heat of formation is not unreasonable. More discussion on this subject is presented in subsection III.3.

The final version of the model was used to reproduce the experimental data (both thermal and chemical activation cases) obtained in argon and nitrogen bath gases. Data fitting procedures were the same as those used for helium bath gas. The contribution of small fractions of the butene component of the bath gas was included via formula XVI. A proportional $\langle\Delta E\rangle_{down}$ vs T dependence was imposed in fitting the thermal decomposition data. The results of the fitting are illustrated in Figures 5−7. Figure 5 displays the fitted $\langle\Delta E\rangle_{down}(Ar)$ and $\langle\Delta E\rangle_{down}(N_2)$ values as functions of temperature. As can be seen from the plots, both dependencies can be represented with linear proportional relationships

$$\langle\Delta E\rangle_{down}(Ar) = 0.674T \text{ cm}^{-1} \qquad (T \text{ expressed in K}) \tag{XVIII}$$

$$\langle\Delta E\rangle_{down}(N_2) = 0.702T \text{ cm}^{-1} \qquad (T \text{ expressed in K}) \tag{XIX}$$

Figures 6 and 7 compare the experimental pressure-dependent data with the results of calculations obtained with the final optimized model and using expressions XVIII and XIX for $\langle\Delta E\rangle_{down}$ vs T dependencies.

Experimental data obtained in chemical activation experiments with Kr, Ne, H_2, D_2, CO_2, CH_4, SF_6, CD_3F, and CH_3Cl as bath gases were also modeled using the final version of the reaction model. The experiments of Kohlmaier and Rabinovitch[9,10] where these bath gases had been used were conducted at room temperature for all of these colliders and also at 195 and 373 K for Kr, Ne, H_2, and D_2. Thermal decomposition data are not available for these bath gases. Therefore, $\langle\Delta E\rangle_{down}$ vs T dependencies obtained from fitting the data carry more limited information compared with the data on He, Ar, and N_2 bath gases. However, qualitatively, the results of fitting exercises for Kr, Ne, H_2, and D_2 are very similar to those obtained with He, Ar, and N_2. $\langle\Delta E\rangle_{down}$ vs T dependencies are best represented with linear proportional functions

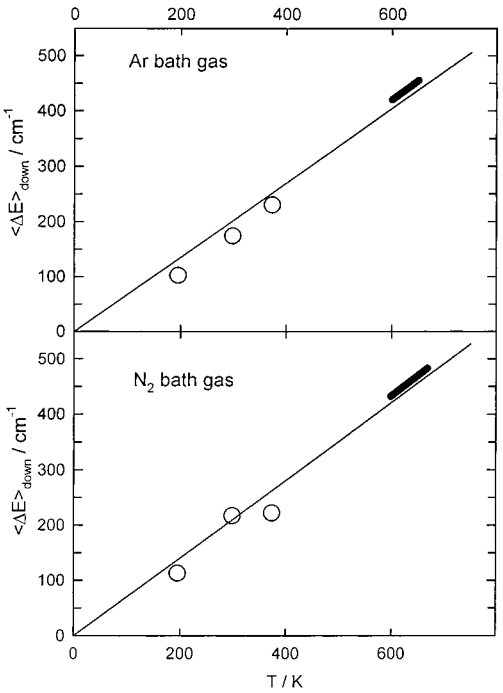

Figure 5. $\langle\Delta E\rangle_{down}$ vs temperature dependencies obtained in fitting experimental falloff data in Ar and N_2 bath gases with the final model. Symbols: $\langle\Delta E\rangle_{down}$ values obtained from fitting data[9,10] on chemically activated reaction. Wide lines: results of modeling of the data[12] on thermal decomposition of *sec*-C_4H_9 radical. Thin lines: linear proportional fits (expressions XVIII and XIX).

$$\langle\Delta E\rangle_{down}(Kr) = 0.594T \text{ cm}^{-1} \qquad (T \text{ expressed in K}) \tag{XX}$$

$$\langle\Delta E\rangle_{down}(Ne) = 0.570T \text{ cm}^{-1} \qquad (T \text{ expressed in K}) \tag{XXI}$$

$$\langle\Delta E\rangle_{down}(H_2 \text{ and } D_2) = 0.482T \text{ cm}^{-1} \qquad (T \text{ expressed in K}) \tag{XXII}$$

Values of $\langle\Delta E\rangle_{down}$ at individual temperatures and comparison of experimental $S/(S + D)$ vs pressure dependencies with those calculated using formulas XX, XXI, and XXII are presented in Table 2 and Figures 8−10. Here, one function (expression XXII) was chosen to represent the $\langle\Delta E\rangle_{down}$ vs T dependence for H_2 and D_2. Results obtained with D_2 (open symbols in the inset in Figure 10) suggest a somewhat steeper than proportional temperature dependence. However, considering the limited amount of experimental data available and the fact that fitted $\langle\Delta E\rangle_{down}$ values for H_2 and D_2 nearly coincide at two of the three temperatures (195 and 298 K), we choose to use a simpler proportional functional form.

Modeling of experimental data obtained in CO_2, CH_4, SF_6, CD_3F, and CH_3Cl bath gases resulted in fitted values of $\langle\Delta E\rangle_{down}$ at room temperature: 239 for CO_2, 269 for CH_4, 301 for SF_6, 327 for CD_3F, and 273 for CH_3Cl. No temperature dependencies could be obtained since only room-temperature experimental data are available. Experimental data are compared with fits in Figure 11.

As can be seen from Figures 1, 2, 4, and 6−11, experimental data are well reproduced by the model. Significant deviations

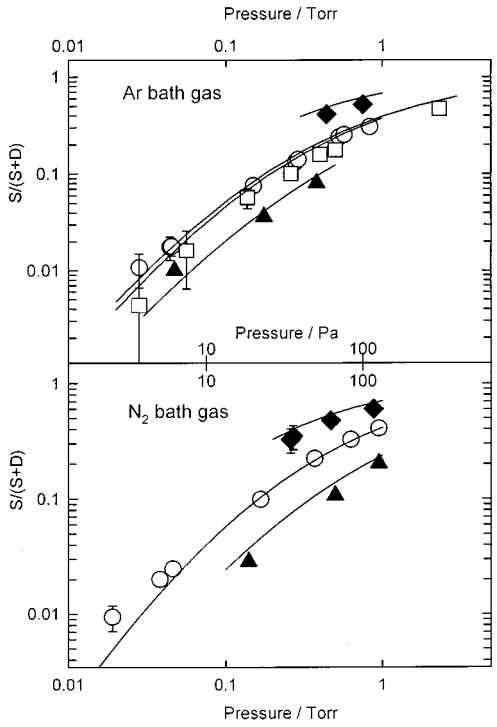

Figure 6. Experimental (symbols) and calculated (lines) pressure dependencies (falloffs) of stabilization branching fractions in the reaction of H atoms with *cis*-C_4H_8 in Ar and N_2 bath gases (with a small fraction of *cis*-C_4H_8, 2.0−4.8%). Experimental data are from Kohlmaier and Rabinovitch.[9,10] Calculated curves are obtained with the final reaction model (see subsection II.3) and $\langle\Delta E\rangle_{down}$ vs T dependencies given by expressions XVIII and XIX. Symbols: triangles (195 K), circles and squares (298 K), and diamonds (373 K). Two types of symbols and two lines at 298 K in the upper plot correspond to two different fractions of *cis*-C_4H_8 in the bath gas: 4.8% (circles) and 2.0% (squares). Experimental uncertainties shown are estimated in the current work from reported[9,10] corrections for "low-pressure artifact"; see text (subsection III.1).

can be observed only in the $S/(S + D)$ vs pressure dependencies at low pressures where experimental data are affected by the "low-pressure artifact" (see subsection II.1 and refs 7−10 for the description of this experimental problem). The magnitudes of deviations between the experimental and calculated dependencies are comparable with the uncertainties of experimental data where the latter could be estimated.

An attempt was made to reproduce the experimental data of Rabinovitch and co-workers[6−10] on H + C_4H_8 reactions obtained with isomers of butene other than *cis*-C_4H_8: *trans*-C_4H_8 and 1-butene. The final model of the reactive system was used without any further modifications. $\langle\Delta E\rangle_{down}$ values for *trans*-C_4H_8 and 1-butene were taken as equal to those obtained for *cis*-C_4H_8 and the $\langle\Delta E\rangle_{down}$ vs T dependence given by expression XVII was used for He as bath gas. The results of modeling are shown in Figures 12 and 13 which demonstrate calculated and experimental values of the stabilization branching fraction ($S/(S + D)$) as functions of pressure for corresponding butenes as bath gases (in the main plots) and for He as bath gas (inset in Figure 12). As can be seen from the plots, while the calculated data for *trans*-C_4H_8 display a reasonable agreement with the experiment (except for the low-pressure part of the main plot in Figure 12, see the "low-pressure artifact" comment above), the results of modeling obtained for 1-butene display a significant deviation from the reported experimental data. A potential reason for this disagreement is that addition of an H atom to 1-butene can occur at both terminal and nonterminal positions (also see Discussion, subsection III.1).

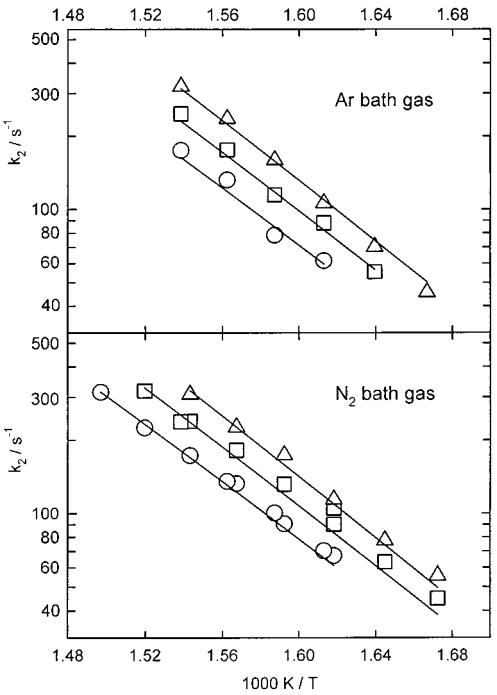

Figure 7. Experimental (symbols) and calculated (lines) rate constants of thermal decomposition of *sec*-C_4H_9 in Ar and N_2 bath gas. Experimental data are from Knyazev et al.[12] Calculated lines are obtained by master equation modeling (current work, final model, $\langle\Delta E\rangle_{down}$ vs T dependencies given by formulas XVIII and XIX). Circles, [M] = 3×10^{16} molecules cm^{-3}; squares, [M] = 6×10^{16} molecules cm^{-3}; triangles, [M] = 12×10^{16} molecules cm^{-3}.

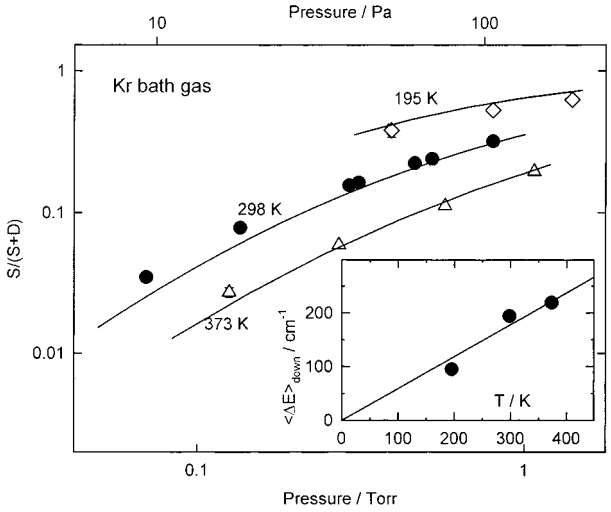

Figure 8. Main plot: experimental (symbols) and calculated (lines) pressure dependencies (falloffs) of stabilization branching fractions in the reaction of H atoms with *cis*-C_4H_8 in Kr bath gas (with a small fraction of *cis*-C_4H_8, 5.4%). Experimental data are from Kohlmaier and Rabinovitch.[9,10] Calculated curves are obtained with the final model (see subsection II.3) and $\langle\Delta E\rangle_{down}$ vs T dependence given by expression XX. Symbols: triangles (195 K), circles (298 K), and diamonds (373 K). Experimental uncertainties shown are estimated in the current work from reported[9,10] corrections for "low-pressure artifact"; see text (subsection III.1). Inset: temperature dependence of $\langle\Delta E\rangle_{down}$(Kr) obtained in modeling the experimental falloffs with the final model.

The final model of reaction 1 was used to calculate stabilization branching fractions, $S/(S + D)$, over wide ranges of temperatures and pressures for helium, argon, and nitrogen bath gases. The results are presented in the Supporting Information. The highest temperature of these calculations, 800 K, was

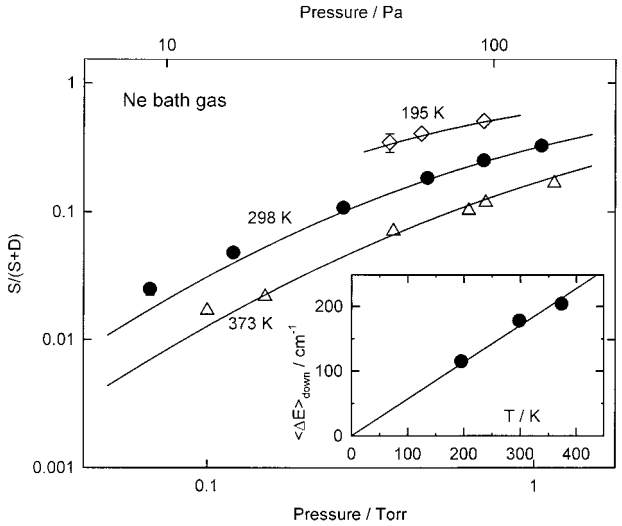

Figure 9. Main plot: experimental (symbols) and calculated (lines) pressure dependencies (falloffs) of stabilization branching fractions in the reaction of H atoms with *cis*-C_4H_8 in Ne bath gas (with a small fraction of *cis*-C_4H_8, 4.4%). Experimental data are from Kohlmaier and Rabinovitch.[9,10] Calculated curves are obtained with the final model (see subsection II.3) and $\langle\Delta E\rangle_{down}$ vs T dependence given by expression XXI. Symbols: triangles (195 K), circles (298 K), and diamonds (373 K). Experimental uncertainties shown are estimated in the current work from reported[9,10] corrections for "low-pressure artifact"; see text (subsection III.1). Inset: temperature dependence of $\langle\Delta E\rangle_{down}$(Ne) obtained in modeling the experimental falloffs with the final model.

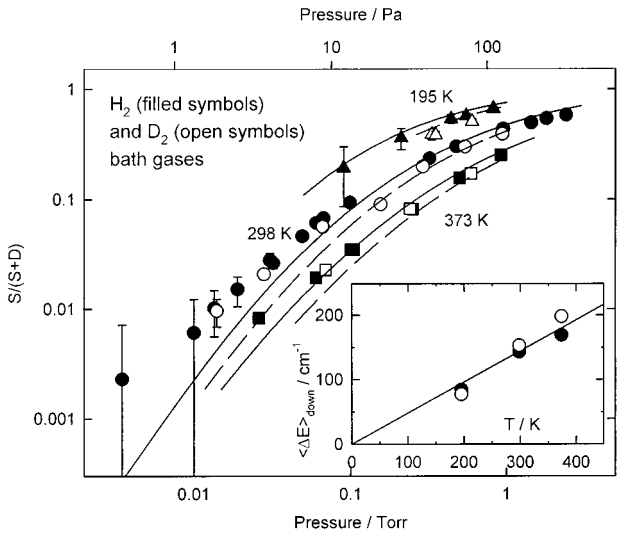

Figure 10. Main plot: experimental (symbols) and calculated (lines) pressure dependencies (falloffs) of stabilization branching fractions in the reaction of H atoms with *cis*-C_4H_8 in H_2 (filled symbols, solid lines) and D_2 (open symbols, dashed lines) bath gases (with a small fraction of *cis*-C_4H_8, 6.1−6.9%). Experimental data are from Kohlmaier and Rabinovitch.[9,10] Calculated curves are obtained with the final model (see subsection II.3) and $\langle\Delta E\rangle_{down}$ vs T dependence given by expression XXII. Symbols: triangles (195 K), circles (298 K), and diamonds (373 K). Experimental uncertainties shown are estimated in the current work from reported[9,10] corrections for "low-pressure artifact"; see text (subsection III.1). Inset: temperature dependencies of $\langle\Delta E\rangle_{down}(H_2)$ and $\langle\Delta E\rangle_{down}(D_2)$ obtained in modeling the experimental falloffs with the final model.

determined by the onset of non-steady-state effects[13,53,55−59] at higher temperatures.

III. Discussion

The current study is the first theoretical modeling work that successfully reproduces two qualitatively different sets of experimental data for the same unimolecular reaction: data obtained in both the chemically and the thermally activated decomposition of secondary butyl radical. The two different ways used to excite the species undergoing decomposition to high vibrational energies sufficient for reaction result in very different activation energy-distribution functions (Figure 14). The fact that one model reproduces pressure dependent data for both methods of activation serves as an indication of the

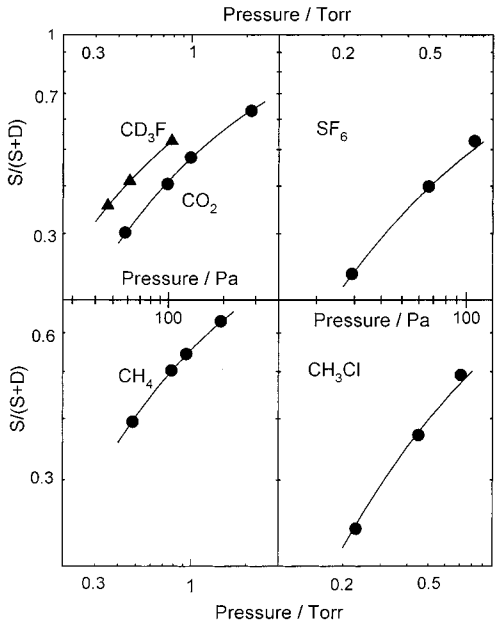

Figure 11. Experimental (symbols) and calculated (lines) room-temperature pressure dependencies of stabilization branching fractions in the reaction of H atoms with *cis*-C_4H_8 in polyatomic bath gases (with a small fraction of *cis*-C_4H_8, 3.3−4.8%). Experimental data are from Kohlmaier and Rabinovitch.[9,10] Calculated curves are obtained with the final model (see subsection II.3).

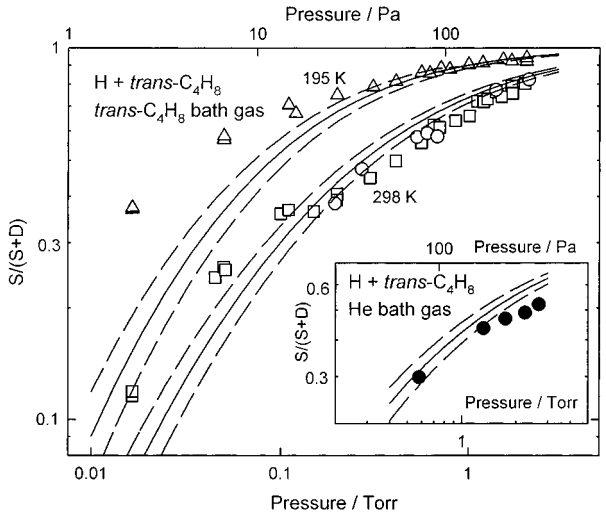

Figure 12. Experimental (symbols) and calculated (lines) pressure dependencies (falloffs) of stabilization branching fractions in the reaction of H atoms with *trans*-C_4H_8 in *trans*-C_4H_8 bath gas (main plot) and in He bath gas with a small fraction (6.0%) of *trans*-C_4H_8 (inset). Experimental data are from Kubin et al.[7,8] (squares and triangles) and Kohlmaier and Rabinovitch[9,10] (circles). Symbols: triangles (195 K), circles and squares (298 K). Solid lines are obtained with the final model (see subsection II.3), values of $\langle\Delta E\rangle_{down}$(*trans*-$C_4H_8$) taken as equal to those of $\langle\Delta E\rangle_{down}$(*cis*-$C_4H_8$), and $\langle\Delta E\rangle_{down}$(He) vs T dependence given by expression XVII. Dashed lines are obtained with the heat of formation of *trans*-C_4H_8 varied by ±1.0 kJ mol^{-1} (see text, subsection III.1).

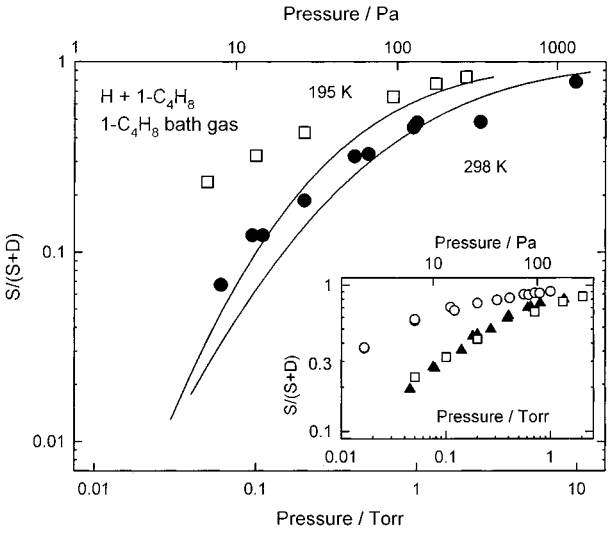

Figure 13. Main plot: experimental (symbols) and calculated (lines) pressure dependencies (falloffs) of stabilization branching fractions in the reaction of H atoms with 1-C_4H_8 in 1-C_4H_8 bath gas. Experimental data are from Kubin et al.[7,8] (open squares, 195 K) and Harrington[6] (filled circles, 298 K). Lines are obtained with the final model (see subsection II.3) and values of $\langle\Delta E\rangle_{down}$(1-$C_4H_8$) taken as equal to those of $\langle\Delta E\rangle_{down}$(*cis*-$C_4H_8$). Inset demonstrates relative (experimental) efficiency of stabilization in the reactions of H atoms with *trans*-C_4H_8 (circles),[7,8] *cis*-C_4H_8 (triangles),[4,9,10] and 1-C_4H_8 (squares)[7,8] at 195 K in butene bath gases. It can be seen that the ordering of relative stabilization efficiencies expected from the reaction energetics is violated: the H + 1-C_4H_8 reaction results in the same stabilization as the H + *cis*-C_4H_8 reaction, while the H + *trans*-C_4H_8 yields the highest stabilization, as expected.

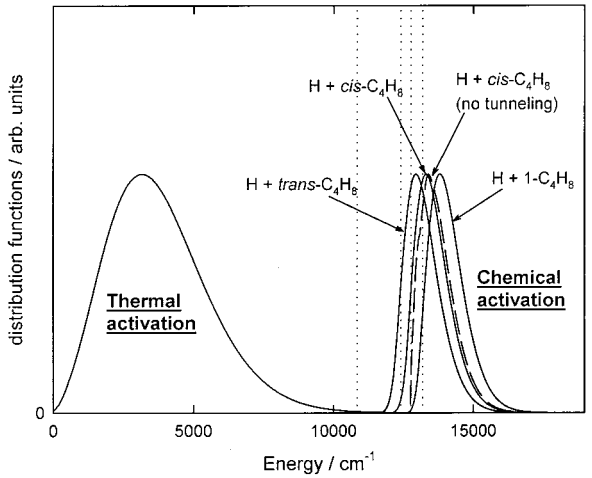

Figure 14. Activation energy-distribution functions corresponding to the conditions of experiments on the thermally activated decomposition[12] of *sec*-C_4H_9 at 640 K and chemically activated H + C_4H_8 reactions at 298 K.[4,6−10] Three different solid lines for the chemical activation distribution correspond to three isomeric versions of the H + C_4H_8 reaction. The influence of tunneling can be seen by comparing the dashed line (obtained for the H + *cis*-C_4H_8 reaction without accounting for tunneling) with the corresponding solid line (obtained with tunneling included). Dotted lines indicate the positions of barriers for reactions 1b, 1at, 1ac, and 1aα. While accurately describing the activation functions, the plot, perhaps, serves to somewhat exaggerate the "distance" between the thermal and the chemical activation cases on the energy scale: the range of energies where collisional energy transfer determines the rate constant in the thermal activation case is located not at the maximum of the thermal activation distribution but in the area around the barrier for channel 1b.

adequacy of the collisional energy transfer description used in modeling and provides further support to the method of modeling of unimolecular reactions given by a combination of RRKM[1−3] theory for microscopic rates and master equation[2,13,53,54] solution for weak-collision pressure effects. In this section, first, the agreement between the experimental and calculated data is discussed in light of the uncertainties of both the experiments and the modeling efforts. Second, qualitative shapes of pressure-dependent falloff curves are considered and a comparison with the frequently used (due to its simplicity) modified strong-collision approximation is reviewed. Third, values and temperature dependencies of $\langle\Delta E\rangle_{down}$ obtained from modeling are discussed.

III.1. Comparison of Experimental and Calculated Pressure Dependencies. As can be seen from plots in Figures 1, 2, 4, 6−12, the agreement between the experimental and the calculated values of stabilization branching ratios and thermal decomposition rate constants is good. Calculated $S/(S + D)$ values deviate systematically from the reported experimental data only in the following cases: (1) at low pressures (below 2.7 Pa (0.02 Torr)) in room-temperature experiments on the H + *cis*-C_4H_8 reaction where *cis*-C_4H_8, He, and H_2 (D_2) bath gases were used (Figures 1, 2, and 10, respectively); (2) at low pressures (below 13 Pa (0.1 Torr)) in 195 K experiments on the H + *trans*-C_4H_8 reaction in *trans*-C_4H_8 bath gas (Figure 12); (3) at pressures below 133 Pa (1 Torr) in the experiments on the H + 1-C_4H_8 reaction (1-butene bath gas, Figure 13). Potential reasons for these disagreements are analyzed below.

At the lowest experimental pressures of Rabinovitch and coworkers, their results were affected by the "low-pressure artifact"[7−10] that manifested itself by producing more stabilization products than can be explained by the kinetic model used by the authors to interpret the product analysis results. Phenomenological correction was used by the authors in some of the experiments to approximately correct low-pressure data for this artifact. We take the values of this correction (where reported) as a measure of experimental uncertainty in individual experiments. These (very approximate) uncertainty values are indicated by error bars in Figures 1, 2, 6, and 8−10. At the lowest pressures in Figures 2 and 10 these uncertainties are so large that they exceed even the corrected values themselves. As can be seen from the plots in Figures 1, 2, and 10, the values of these uncertainties are comparable with the deviations between the experimental and calculated $S/(S + D)$ branching ratio values. Therefore, the observed low-pressure differences between the theory and the experiment can be explained by experimental uncertainties and do not serve as an indication of failure of theory.

An additional factor potentially contributing to the low-pressure deviations between the calculated and the experimental pressure dependencies is due to the fact that at the lowest pressures of the experiments of Rabinovitch and co-workers the frequency of collisions with the reactor wall becomes a noticeable fraction of the overall collision frequency. For example, at 0.52 Pa (0.0039 Torr) of He in the experiments of Kohlmaier and Rabinovitch,[9,10] collisions with the wall constitute 3.5% of the collisions with the bath gas (the wall collision frequency is estimated as $^1/_4\bar{v}$**S**[M], where $\bar{v}$ is the average thermal molecular velocity and **S** is the reactor surface). Considering their potentially higher energy transfer efficiency, wall collisions (unaccounted for in the current modeling efforts) can thus result in an increase of the stabilization branching fraction compared to the purely homogeneous system.

The deviation between the experimental and the calculated $S/(S + D)$ vs pressure dependencies for the H + *trans*-C_4H_8 reaction in *trans*-C_4H_8 bath gas at 195 K is larger (Figure 12)

than that observed in the case of the H + *cis*-C_4H_8 reaction (Figure 1) and has its origin at higher pressures. The experimental data presented in Figure 12, however, are of lower precision than those in Figure 1. The 298 K data, although reported in the Ph.D. thesis of Kubin,[8] are not presented in the journal article[7] based on the thesis (only the high-pressure limiting result is presented in Table 6 of ref 7). Also, the authors of the article explicitly assert that the data are affected by the "low-pressure artifact" and that, specifically, the 195 K H + *trans*-C_4H_8 results can be of doubtful validity even at high pressures.

Computational simulation of the H + *trans*-C_4H_8 system can be affected by an additional uncertainty of the model. The final model described in subsection II.3 was tuned (by adjusting $\langle\Delta E\rangle_{down}$ and $\Delta_f H°_{298}$(*sec*-C_4H_9) values) to reproduce the H + *cis*-C_4H_8 experimental data. The heat of formation of *trans*-C_4H_8, however, is known with an uncertainty of ±1.0 kJ mol^{-1}.[38,39] This uncertainty propagates into the uncertainty in the energy difference between the H + *cis*-C_4H_8 and the H + *trans*-C_4H_8 "entrance" channels of chemical activation. Thus, although the model should describe the H + *cis*-C_4H_8 results exactly, the calculated H + *trans*-C_4H_8 stabilization branching factions are influenced by the $\Delta_f H°_{298}$(*trans*-C_4H_8) uncertainty. This effect is illustrated in Figure 12 where dashed lines indicate the $S/(S + D)$ pressure dependencies obtained using the final model but with the *trans*-C_4H_8 heat of formation varied by ±1.0 kJ mol^{-1}. An additional, not easily estimated, uncertainty derives from the fact that $\langle\Delta E\rangle_{down}$ for *trans*-C_4H_8 as bath gas, taken here as equal to those of *cis*-C_4H_8, can in reality be different.

The largest disagreement between theory and experiment is observed in the case of the H + 1-C_4H_8 reaction (Figure 13). Here, both the experimental data and the critical model parameters are of questionable reliability because they were obtained under the assumption that only secondary butyl radicals are formed in the addition step of the overall reaction. However, only the terminal addition will form secondary butyl radical, while the nonterminal process will result in the formation of normal butyl radical. Rabinovitch and co-workers assumed that only the terminal process is important in their experiments and, consequently, analyzed the products within the resultant kinetic model. In the current work, the model of the reactive system given by (1) was created under the same assumption, following Rabinovitch and co-workers. In fact, as data tables in refs 6 and 8 indicate, in the experiments on the H + 1-butene reaction substantial amounts of C_2H_4 were formed, exceeding the yields of ethylene observed in reactions of H atoms with other butene isomers under similar conditions. This production of C_2H_4 can serve as an indication of the importance of the formation of chemically activated *n*-C_4H_9 radical which decomposes into C_2H_5 and C_2H_4. No independent direct experimental assessments of terminal vs nonterminal addition processes in the H + 1-butene reaction are available in the literature.

The experimental data on the H + 1-butene reaction at 298 K presented in Figure 13 are taken from the Ph.D. thesis of Harrington[6] (these data, cited in ref 11, were not published in any journal article). The 195 K data are taken from the Ph.D. thesis of Kubin.[8] In the journal article based on this thesis work, Kubin, Rabinovitch, and Harrington[7] present only the three data points corresponding to the high-pressure end of the experimental range since they consider the lower-pressure data unreliable due to the "low-pressure artifact."

Because 1-C_4H_8 has the highest heat of formation compared to the *cis*- and *trans*-butenes, the H + 1-C_4H_8 "entrance" channel is characterized by the highest energy of the initially formed activated *sec*-C_4H_9 radicals (Figure 14). Therefore, when comparing the $S/(S + D)$ vs pressure curves obtained in the reactions of H atoms with the three butene isomers, one can expect to see the highest fraction of stabilization in the case of *trans*-C_4H_8 (lowest heat of formation), intermediate stabilization in the case of *cis*-C_4H_8 (intermediate heat of formation), and the lowest stabilization fraction in the H + 1-C_4H_8 case. However, as can be seen from the plot in the inset of Figure 13, this ordering of relative stabilization efficiencies is violated at 195 K: H + 1-C_4H_8 reaction results in the same stabilization as the H + *cis*-C_4H_8 reaction, while the H + *trans*-C_4H_8 yields highest stabilization, as expected. The above discussion serves to demonstrate that deviations between theory and experiment are only observed in cases where experimental data are suspect.

III.2. Shapes of Pressure Dependent (Falloff) Curves in Chemically Activated Reactions. *Comparison with Modified Strong Collision Approximation.* The qualitative behavior of pressure dependencies of chemically activated reactions in the case of weak collisions with the bath gas has been described by Rabinovitch and co-workers.[4,9] In the current subsection we expand this description and compare the falloff shapes obtained under the weak collision assumption with those calculated using the popular modified strong collision approximation.

In the most simplified, Lindemann-type model of pressure effects, where the molecule is considered to be in one of two possible states (activated or deactivated) and each collision with the bath gas deactivates an activated molecule, the ratio of decomposition to stabilization rates will be equal to

$$\frac{D}{S} = \frac{k}{\omega} \qquad \text{(XIII)}$$

Here, k is the rate of decomposition of an activated molecule and ω is the frequency of collisions with the bath gas. For the more complex (and more realistic) case of energy-dependent microscopic rate constants Rabinovitch and Diesen[4] proposed to use an effective, or "intuitive" decomposition rate constant obtained via expression XXIII from the collision frequency and D/S ratio for the purpose of analyzing shapes of pressure dependencies:

$$k_a = \omega\frac{D}{S} \qquad \text{(XXIV)}$$

k_a does, indeed, present a convenient means of analysis since it removes from the pressure dependence its dominating Lindemann-type component. While the scales of changes in D/S or $S/(S + D)$ are comparable with the scale of changing pressure, k_a is less dependent on pressure. In fact, all pressure dependence of k_a occurs due to deviation from the Lindemann behavior.

Figure 15 presents shapes of falloff curves and corresponding k_a vs pressure dependencies for chemically activated decomposition of secondary butyl radical (H + *cis*-C_4H_8 is the activating reaction) in He bath gas at 650 K obtained using the final model developed in the current work. The weak collision case with $\langle\Delta E\rangle_{down}$ given by formula XVII is represented by the solid line and the modified strong collision approximation by the dashed line. Formulas for $S/(S + D)$ vs pressure dependence for the modified strong collision case can be found, for example, in refs 3 and 9. The collision efficiency $\beta_c = 0.0775$ and factor $F_E = 1.940$ for the modified strong collision case were computed via formulas 2.31 and 4.8 of ref 80, respectively. As can be seen from the plots, the modified strong collision approximation yields a very poor representation of the weak collision falloff, with differences being as large as several orders of magnitude.

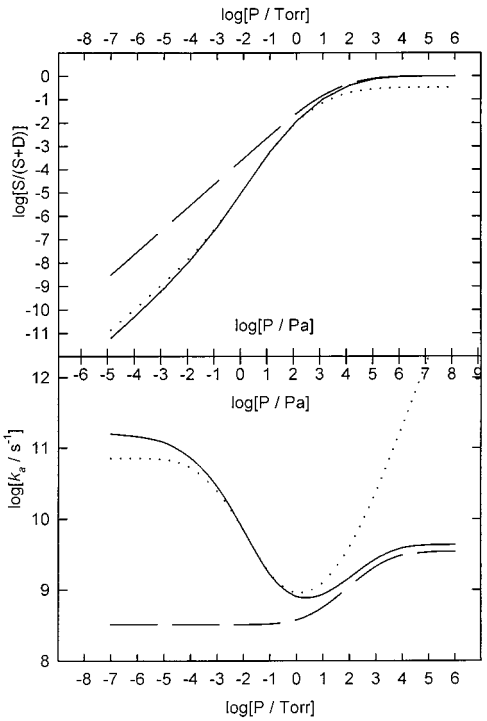

Figure 15. Stabilization falloff curves (upper plot) and k_a vs pressure dependencies (lower plot) calculated for He bath gas at 650 K using the final reaction model and (1) exponential-down weak collision model with *virtual component* formalism,[13] solid lines, (2) modified strong collision model, dashed lines, and (3) exponential-down weak collision model with stabilization and decomposition channel fractions obtained via "straightforward" integration of fluxes (at fixed time of 10^{-3} s; see text, subsection III.2), dotted lines. Large deviations between the weak collision and the modified strong collision models demonstrate the inapplicability of the modified strong collision model to chemically activated systems. Deviations between the solid and the dotted lines illustrate the fact that, at higher temperatures, caution must be exercised to select time corresponding to the correct steady state when applying the "straightforward" flux-integration approach to computation of branching fractions.

Recently, Venkatesh et al.[81] observed large deviations between the results obtained with weak collision and modified strong collision models in their master equation calculations of the $HO_2 + C_2H_4$ channel fractions in the reaction of C_2H_5 with O_2. When considering these results, one should bear in mind that formulas used for β_c and F_E were developed by the authors of ref 80 for thermally activated reactions only and were not intended for use in chemical activation cases. These formulas, however, are frequently used for this purpose by other workers in practical calculations.

At 650 K the thermal decomposition of *sec*-C_4H_9 is important (This temperature was chosen to accentuate the effects of the thermal reaction.). The *virtual component* formalism[13] used in the current work takes thermal decomposition into account since this method distinguishes between the decomposition of *sec*-butyl radicals that are activated chemically from the decomposition of those radicals that were stabilized by collisions and then thermally reactivated. An alternative, "straightforward" way of computing rates of decomposition and stabilization can be based on averaging (by integration) of microscopic rates $k(E)$ over the steady-state population distribution (to determine D, the decomposition flux) and by computing the overall flux of activated molecules "downward" along the energy axis (to determine S). The results of the *virtual component* approach and of the alternative, "straightforward" method coincide if steady state[53,54] is achieved. However, at higher temperatures, a second steady state appears due to the thermal decomposition of the stabilized adduct.[53] Under such conditions, the correct identification of the first and the second steady states is imperative for the "straightforward" method; fluxes must be computed at a reaction time corresponding to the first steady state. If the correct time is not selected, the "straightforward" method fails to describe the thermal reactivation of the stabilized molecules as a separate phenomenon and yields incorrect values of reaction branching fractions and k_a (dotted lines in Figure 15 indicate incorrect pressure dependencies obtained via the "straightforward" method by setting a fixed time of 10^{-3} s for all pressures).

Other methods of the master equation solution and its interpretation for chemically activated reactions have been published in the literature (see for example, refs 54, 93−95). All of these works are based on the same fundamental understanding of the physics of processes occurring in reactive systems characterized by chemical activation. At the same time, the numerical methods used by these authors differ. A discussion of different approaches to the master equation solution can be found in ref 95. Earlier work by Smith et al.[54] provided a solution for the steady-state case. Later studies concentrated on solving the time-dependent master equation and providing solutions in the form of complex concentration vs time dependencies, including cases of non-steady-state behavior. Derivation of rate constant values from such solutions would be similar to the "straightforward" method described above in the sense that careful identification of the time interval corresponding to the appropriate steady state is required for the results to be meaningful. The *virtual components* formalism[13] used in this study provides formulas both for the steady-state rate constants (without need for explicit consideration of time dependencies) and the solution for non-steady-state kinetics that allows its incorporation into large-scale kinetic schemes.

The qualitative behavior of the k_a vs pressure dependence has been discussed earlier by Diesen and Rabinovitch[4] and by Kohlmaier and Rabinovitch.[9,10] The increase of k_a with pressure at the high-pressure end of the dependence (present in both cases of weak and strong collision) is due to the nonzero width of the activation distribution (energy distribution of the molecules formed in the activating reaction).[3,4] In the strong collision case, $k_a = \langle k(E) \rangle$ in the high-pressure limit and $k_a = (\langle k(E)^{-1} \rangle)^{-1}$ in the low-pressure limit, where averaging is done over the activation distribution.[3,4,9,14] Therefore, one can expect an increase with temperature of the relative difference between the intermediate-pressure and the high-pressure k_a values due to the widening of the activation distribution.

The increase of k_a with decreasing pressure observed only in the weak collision case is due to the fact that, effectively, several collisions are required to deactivate an excited molecule to a level below the barrier to decomposition. At low pressures, such multistep deactivation decreases at a rate faster than proportional to pressure, stabilization shows a steeper than proportional pressure dependence, and k_a increases with pressure.[9,10] In the low-pressure limit k_a becomes pressure independent and the stabilization rate becomes proportional to pressure. This regime occurs when the pressure is too low for multistep deactivation and all stabilization is due to an extremely inefficient one-step deactivation on the "tail" of the collision energy transfer probability function. Thus, the low-pressure limiting value of k_a is most sensitive to the energy difference between the critical energies of the "entrance" and the "exit" channels of a chemically activated reaction and to the long-range part of the collisional energy transfer probability function $P(E,E')$. In

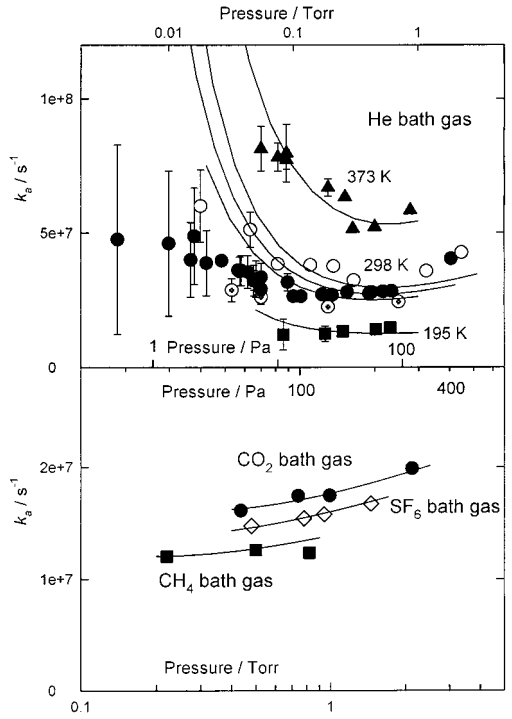

Figure 16. Selected experimental and calculated pressure dependencies of k_a. Upper plot: He bath gas (with small fractions of *cis*-C_4H_8). Lower plot: CO_2, CH_4, and SF_6 bath gases. Sources of experimental data and symbols are the same as in Figures 2 and 11.

particular, effects of "supercollisions" (collisions that transfer large amounts of vibrational energy) can be expected to play a role in this low-pressure regime. Although a recent direct experimental study of collisional energy transfer puts the fraction of "supercollisions" at less than 1%,[74] considering the several orders of magnitude of difference between the k_a values at low and intermediate pressures, one can expect that even this small fraction can affect the low-pressure k_a values. In the current example, the low-pressure proportional regime (k_a = constant) is reached only at physically impractical pressures ($<10^{-4}$ Pa ($<10^{-6}$ Torr)), where collisions with reactor walls will dominate over collisions with the bath gas). For other reactions with a lower energy gap between the "entrance" and "exit" channels this regime may become practically achievable.

Kohlmaier and Rabinovitch[9,10] used the experimental k_a vs pressure dependencies and, in particular, the "turnup" of k_a at low pressures to evaluate parameters of weak collisions with the bath gas. However, at these low pressures the accuracy of experimental data was the lowest (see subsections II.1 and III.1). Intermediate and high experimental pressures corresponded to the regime where k_a does not significantly change with pressure, with the exception of data obtained in polyatomic bath gases, which show an increase in k_a with pressure. Therefore, in the current work, we prefer to use the overall agreement between the experimental and calculated $S/(S + D)$ vs pressure curves to derive information on $\langle\Delta E\rangle_{down}$ rather than accentuate the low-pressure experimental k_a behavior. For illustrative purposes, Figure 16 demonstrates the (rather uncertain at low pressures) experimental and calculated k_a vs pressure dependencies for He, CO_2, CH_4, and SF_6 bath gases.

III.3. Values and Temperature Dependencies of $\langle\Delta E\rangle_{down}$. The values of $\langle\Delta E\rangle_{down}$ obtained in the fitting of the experimental data demonstrate strong positive temperature dependencies. In the modeling process, first, a linear proportional dependence was obtained by fitting the experimental $S/(S + D)$ vs pressure curves reported by Kohlmaier and Rabinovitch[9,10] for He as bath gas. Second, this simple functional form ($\langle\Delta E\rangle_{down}$ proportional to T) was assumed to extend to higher temperatures corresponding to the experimental conditions of the thermal decomposition experiments of Knyazev et al.[12] Thus, a linear proportional temperature dependence of $\langle\Delta E\rangle_{down}$ was artificially imposed in the process of modeling the thermal decomposition data. Third, the model was adjusted (correction of -3.4 kJ mol^{-1} was applied to $\Delta_fH°_{298}$(*sec*-C_4H_9)) so that $\langle\Delta E\rangle_{down}$ vs T dependencies obtained via fitting chemical activation data and thermal decomposition data in He coincide (subsection II.3). This exercise yielded $\langle\Delta E\rangle_{down} = 0.520T$ cm^{-1} (expression XVI, T expressed in K) for He as bath gas. Finally, the adjusted model was used to simulate experimental data on both the chemically[3,4,6−10] and thermally[12] activated decomposition of secondary butyl radical in other bath gases.

Fitting of falloff data for other bath gases performed without any further modifications of model yielded similar linear proportional temperature dependencies of $\langle\Delta E\rangle_{down}$ for all small (monatomic and diatomic) colliders for which temperature-dependent data are available. These temperature dependencies are given by expressions XVII−XXII and illustrated in Figures 3, 5, 8−10. For two of the bath gases, Ar and N_2, these temperature dependencies were derived from thermal decomposition data as well as from the results of experiments on the chemically activated reaction (Figure 5). The only polyatomic bath gas for which temperature-dependent data are available, *cis*-C_4H_8, demonstrates an even stronger than proportional temperature dependence of $\langle\Delta E\rangle_{down}$ (inset in Figure 1).

Since the proportionality coefficients of the fitted $\langle\Delta E\rangle_{down}$ vs T dependencies are very sensitive to some of the critical parameters of the model (for example, to $\Delta_fH°_{298}$(*sec*-C_4H_9), as demonstrated in subsection II.3), it is important to know whether that functional (proportional) form of $\langle\Delta E\rangle_{down}$ vs T is preserved when model parameters are varied within reasonable uncertainties. It is impractical to investigate the influence of all model parameter uncertainties on the fitting results due to their large number. However, we performed an uncertainty analysis for the most important of these parameters.

The influence of the heat of formation of secondary butyl radical on the fitting results is described in subsection II.3 where it is demonstrated that, although variation of $\Delta_fH°_{298}$(*sec*-C_4H_9) results in significant changes of the fitted $\langle\Delta E\rangle_{down}$ vs T dependence, the proportional functional form is preserved. One should note here that although the value of $\Delta_fH°_{298}$(*sec*-C_4H_9) = 64.1 kJ mol^{-1} selected for use in the model was obtained by adjusting the value reported by Seakins et al.[37] by 3.4 kJ mol^{-1}, this new value should not be understood as a more accurate determination of $\Delta_fH°_{298}$(*sec*-C_4H_9). In principle, the values of $\langle\Delta E\rangle_{down}$ obtained from data fitting are very sensitive to the heat of formation of *sec*-butyl radical and the requirement that the $\langle\Delta E\rangle_{down}$(He) vs T dependencies obtained from modeling of the chemical activation and the thermal activation data coincide puts strict boundaries on the value of $\Delta_fH°_{298}$(*sec*-C_4H_9). However, many additional sources of uncertainties in the model parameters (vide infra) influence the $\langle\Delta E\rangle_{down}$ temperature dependencies and, therefore, these parameter uncertainties propagate into the uncertainty of the optimum value of $\Delta_fH°_{298}$(*sec*-C_4H_9).

Another most important parameter to which the modeling results are very sensitive is the energy gap between the barriers for the "entrance" and "exit" channels of the chemically activated reaction. Varying this energy gap in the model has the effect of "shifting" the $k_{1b}(E)$ dependence along the energy scale relative to the energy distribution of chemically activated

sec-butyl radicals and thus modifying the relative efficiency of decomposition vs stabilization.

Several model parameters can contribute to uncertainty in the value of this energy gap. These are the heats of formation of C_4H_8 and C_3H_6 and the activation energies of the high-pressure-limit rate constants of the $H + C_4H_8$ and $CH_3 + C_3H_6$ addition reactions. The first three of these parameters have uncertainties of ± 1.0, ± 0.8, and ± 0.7 kJ mol^{-1}, respectively. The uncertainty in the $CH_3 + C_3H_6 \rightarrow$ *sec*-C_4H_9 reaction activation energy is not easily evaluated since expression I for the temperature dependence of k^{∞}_{-1b} was obtained[12] in an analysis of relative rate measurements of two different groups.[31,32] Considering the fact that these two relative rate measurements agree very well despite using different reference reactions and that they agree with the results of Baldwin et al.,[33] we estimate an upper limit to the uncertainty in the reaction 1b activation energy to be ± 2.0 kJ mol^{-1}. If all the above uncertainties are combined by simple addition, one obtains the maximum possible deviation of ± 4.5 kJ mol^{-1} from the optimum value of the energy gap between the "entrance" and the "exit" channels.

Modeling and fitting of experimental $S/(S + D)$ vs pressure data of Kohlmaier and Rabinovitch[9,10] obtained in He bath gas was repeated twice with the final model described in subsection II.3 modified by increasing or decreasing the above four parameters (heats of formation and energy barriers) in such a way as to provide 4.5 kJ mol^{-1} change in the "entrance-exit" energy gap in both "plus" and "minus" directions. To perform data fitting in He bath gas, first, $\langle \Delta E \rangle_{down}$ values for *cis*-C_4H_8 bath gas had to be obtained with the modified reaction models. The results of this modeling exercise demonstrated that although the individual fitted values of $\langle \Delta E \rangle_{down}$ changed drastically with the variation of the energy gap between the "entrance" and the "exit" channels (reactions -1a and 1b), the proportional $\langle \Delta E \rangle_{down}$(He) vs T dependence was preserved. In particular, $\langle \Delta E \rangle_{down}$(He, plus) $= 1.01T$ cm^{-1} and $\langle \Delta E \rangle_{down}$(He, minus) $= 0.274T$ cm^{-1} (T expressed in K) dependencies were obtained with the increased and decreased energy gaps, respectively. Individual $\langle \Delta E \rangle_{down}$ values obtained for He and *cis*-C_4H_8 bath gases are listed in the Supplement. These results serve to demonstrate that reasonable modifications of the reaction model, while resulting in changes to the fitted $\langle \Delta E \rangle_{down}$ values, do not change the fact of linear direct proportionality in the $\langle \Delta E \rangle_{down}$ vs T dependence observed for small bath gas colliders.

The observed proportionality of the $\langle \Delta E \rangle_{down}$ vs temperature dependence is not surprising. A similar dependence $\langle \Delta E \rangle_{down}$(He) $= 0.255T$ cm^{-1} was derived[76,77] from RRKM/master equation modeling of experimental falloff data on reactions 3 and -3

$$C_2H_5 \leftrightarrow H + C_2H_4 \qquad (3,-3)$$

obtained at temperatures ranging from 298 to 1100 K. Modeling of two other radical decomposition reactions (i-$C_3H_7 \leftrightarrow H + C_3H_6$,[78] $C_2H_3 \leftrightarrow H + C_2H_2$)[46] resulted in a positive temperature dependence of $\langle \Delta E \rangle_{down}$, although with different functional forms. A positive temperature dependence of $\langle \Delta E \rangle_{down}$ is supported by the results of experimental[82] and trajectory[83] studies of collisional energy transfer in large polyatomic molecules. Dashevskaya et al.[84] predict an increase of $\langle \Delta E \rangle_{down}$ with temperature (although less steep than a proportional dependence) within the framework of the sequential direct encounter model. On the other hand, theoretical results of Borjesson and Nordholm[85] and Ming et al.[86] support an opposite, weak negative temperature dependence of $\langle \Delta E \rangle_{down}$ or a $\langle \Delta E \rangle_{down}$ approximately independent of temperature.

The values of $\langle \Delta E \rangle_{down}$ obtained in the current work differ significantly from those derived by Kohlmaier and Rabinovitch[9,10] from the analysis of their experimental data. These authors reported significantly larger average energies transferred per collision, on the order of 400$-$1200 cm^{-1} for small collider molecules and $>$3000 cm^{-1} for polyatomic bath gases. Several factors contributed to the differences, including methods of master equation solution, properties of molecules and transition states involved, methods of data interpretation, etc. One of the sources of disagreement is in the different values of the energy gap between the entrance and the exit channels of the chemically activated reaction. The values of 29$-$33 kJ mol^{-1} were used in refs 9 and 10 while in the current work the lower value of 23 kJ mol^{-1} was used, which was, in addition, somewhat lowered by the tunneling effects (see Figure 14). Most of thermochemical data used in the current work were not available in 1963 when refs 9 and 10 were published.

It is interesting to note that the values of $\langle \Delta E \rangle_{down}$ for relaxation of secondary butyl radical in He, Ar, and CO_2 bath gases obtained in the current work from modeling of kinetic data are reasonably close to those reported in a recent study of Hold et al.[74] These authors applied the most direct of the currently existing experimental techniques, kinetically controlled selective ionization method (KCSI),[74] to monitor the temporal evolution of energy distribution functions in toluene and azulene molecules excited to high vibrational energies. The values of $\langle \Delta E \rangle_{down}$ reported by Hold et al. for He, Ar, and CO_2 differ from those derived in the current work by factors ranging from 0.8 to 1.4: (values are given in cm^{-1} in the following order: this work/ref 74 for toluene/ref 74 for azulene) 158/126/123 (He), 174/173/177 (Ar), 239/272/333 (CO_2). A larger difference is observed for *cis*-C_4H_8 as bath gas: 327/559/642. All $\langle \Delta E \rangle_{down}$ values are for the energy of the reaction 1b barrier (see subsection II.3).

When comparing the above values of $\langle \Delta E \rangle_{down}$ and their temperature dependencies with the results of spectroscopic experiments on collisional relaxation of highly vibrationally excited molecules or with the predictions of trajectory calculations, one should bear in mind that the numerical values of $\langle \Delta E \rangle_{down}$ derived here or elsewhere are obtained through a prism of theory applied to interpret concrete experimental or computational results. Details of the model used translate into the $\langle \Delta E \rangle_{down}$ values. This dependence on the theory used is expected to be more pronounced when collisional energy transfer properties are derived from modeling reaction rate data compared to more direct experimental techniques, such as, for example, the KCSI method.[74] In particular, even considering the large amount of experimental data of different types that were quantitatively described in the current modeling effort, we still cannot discern such details of $P(E,E')$ as the energy dependence of $\langle \Delta E \rangle_{down}$ (assumed here to be linear, formula XV) or the functional form of $P(E,E')$ (assumed to be exponential-down, formula XIV). The real $P(E,E')$ functional form may be different. For example, a noticeable long-range "supercollision" contribution to $P(E,E')$ has been predicted theoretically[87$-$89] and observed experimentally,[74,90] although assessments of the relative importance of such collisions that transfer a large amount of energy differ. Trajectory calculations[87$-$89] predict a substantially more pronounced "supercollision" fraction than do KCSI experiments[74] and state-to-state statistical-dynamical theory.[91] The linear proportional temperature dependence of $\langle \Delta E \rangle_{down}$ observed in the current work may

acquire a different functional form if other models of collisional energy transfer (such as, for example, a biexponential model incorporating a "supercollision" contribution) are used.

In addition, the current model is based on the assumption that the proportional $\langle\Delta E\rangle_{\text{down}}$ vs temperature dependence observed at low temperatures will be sustained above 373 K, up to the temperatures of the experiments of ref 12. It is possible, however, that, with the increase of temperature, $\langle\Delta E\rangle_{\text{down}}$ will stabilize at some constant value. Such stabilization has been invoked before in modeling unimolecular reactions. In his RRKM analysis of the decomposition and formation of simple alkanes in argon bath gas, Tsang[92] has observed that experimental literature data are best reproduced by using values of $\langle\Delta E\rangle_{\text{down}}$ that increase with temperature at low and moderate temperatures but stabilize to a 600 cm^{-1} plateau under combustion conditions.

The success of the current modeling of a very diverse set of kinetic data obtained in two types of experiments characterized by distinctly different shapes of energy distribution functions (chemical and thermal activation) demonstrates the capabilities of statistical theories of unimolecular reactions and the adequacy of the applied master equation description of pressure effects. To further the reliability and predictive abilities of theory, more certain knowledge of collisional energy transfer properties is required and the effects of different features of *P(E,E′)* on chemical kinetics need to be investigated.

Acknowledgment. This research was supported by the National Science Foundation, Combustion and Thermal Plasmas Program under Grant No. CTS-9729287 and by Division of Chemical Sciences, Office of Basic Energy Sciences, Office of Energy Research, U.S. Department of Energy under Grant No. DE-FG02-94ER1446.

Supporting Information Available: Results of the ab initio study of reactions 1ac, 1at, 1aα, and 1b, the results of fitting experimental data with "plus" and "minus" modified models, and the tabulated stabilization branching fractions obtained over wide ranges of pressure and temperature using the final model. Tables 1S and 2S containing information on the properties of several conformations on the potential energy surface. Figures 1S and 2S describing potential energy profiles obtained in IRC following. Table 3S containing the results of data fitting. Tables 4S−6S containing the $S/(S + D)$ values as functions of pressure and temperature calculated in this work for helium, argon, and nitrogen bath gases. Table 7S containing modified Arrhenius fits of individual reaction channel rate constants. This material is available free of charge via the Internet at http://pubs.acs.org.

References and Notes

(1) Forst, W. *Theory of Unimolecular Reactions*; Academic Press: New York, 1973.

(2) Gilbert, R. G.; Smith S. C. *Theory of Unimolecular and Recombination Reactions*; Blackwell Scientific Publications: Oxford, 1990.

(3) Robinson, P. J.; Holbrook, K. A. *Unimolecular Reactions*; Wiley: New York, 1972.

(4) Rabinovitch, B. S.; Diesen, R. W. *J. Chem. Phys.* **1959**, *30*, 735.

(5) Harrington, R. F.; Rabinovitch, B. S.; Diesen, R. W. *J. Chem. Phys.* **1960**, *32*, 1245.

(6) Harrington, R. F. Ph.D. thesis, University of Washington, 1960.

(7) Kubin, R. F.; Rabinovitch, B. S.; Harrington, R. E. *J. Chem. Phys.* **1962**, *37*, 937.

(8) Kubin, R. F. Ph.D. thesis, University of Washington, 1961.

(9) (a) Kohlmaier, G. H.; Rabinovitch, B. S. *J. Chem. Phys.* **1963**, *38*, 1692. (b) Kohlmaier, G. H.; Rabinovitch, B. S. *J. Chem. Phys.* **1963**, *38*, 1709.

(10) Kohlmaier, G. H. Ph.D. thesis, University of Washington, 1962.

(11) Rabinovitch, B. S.; Kubin, R. F.; Harrington, R. E. *J. Chem. Phys.* **1963**, *38*, 405.

(12) Knyazev, V. D.; Dubinsky, I. A.; Slagle, I. R.; Gutman, D. *J. Phys. Chem.* **1994**, *98*, 11099.

(13) Knyazev, V. D.; Tsang, W. *J. Phys. Chem.* **1999**, *103*, 3944.

(14) Rabinovitch, B. S.; Setser, D. W. *Adv. Photochem.* **1964**, *3*, 1.

(15) Rabinovitch, B. S.; Flowers, M. C. *Quart. Rev.* **1964**, *18*, 122.

(16) Harris, G. W.; Pitts, J. N., Jr. *J. Chem. Phys.* **1982**, *77*, 3994.

(17) Kyogoku, T.; Watanabe, T.; Tsunashima, S.; Sato, S. *Bull. Chem. Soc. Jpn.* **1983**, *56*, 19.

(18) Canosa, C. E.; Marshall, R. M.; Sheppard, A. *Int. J. Chem. Kinet.* **1981**, *13*, 295.

(19) Knyazev, V. D.; Dubinsky, I. A.; Slagle, I. R.; Gutman, D. *J. Phys. Chem.* **1994**, *98*, 5279.

(20) Bryukov, M. G.; Slagle, I. R.; Knyazev, V. D. *J. Phys. Chem.*, submitted.

(21) Chen, Y.; Rauk, A.; Tschuikow-Roux, E. *J. Phys. Chem.* **1990**, *94*, 6250. Erratum. *J. Phys. Chem.* **1992**, *96*, 6854.

(22) Zakharieva-Pencheva, O.; Förster, H. *Vibr. Spectrosc.* **1991**, *2*, 227.

(23) Durig, J. R.; Compton, D. A. C. *J. Phys. Chem.* **1980**, *84*, 773.

(24) Chase, M. W., Jr.; Davies, C. A.; Downey, J. R., Jr.; Frurip, D. J.; McDonald, R. A.; Syverud, A. N. *JANAF Thermochemical Tables, Third Edition*, *J. Phys. Chem. Ref. Data* **1985**, *14*, Supplement No. 1.

(25) Chao, J.; Zwolinski, B. J. *J. Phys. Chem. Ref. Data* **1975**, *4*, 251.

(26) Kondo, S.; Hirota, E.; Morino, Y. *J. Mol. Spectrosc.* **1968**, *28*, 471.

(27) Murcko, M. A.; Castejon, H.; Wilberg, K. B. *J. Phys. Chem.* **1996**, *100*, 16162.

(28) Durig, J. R. *J. Chem. Phys.* **1979**, *70*, 5747.

(29) Engeln, R.; Reuss, J. *Chem. Phys.* **1991**, *156*, 215.

(30) Reid, R. C.; Prausnitz, J. M.; Sherwood, T. K. *The Properties of Gases and Liquids*, 3rd ed.; McGraw-Hill: New York, 1977.

(31) Miyoshi, M.; Brinton, R. K. *J. Chem. Phys.* **1962**, *36*, 3019.

(32) Cvetanovic, R. J.; Irwin, R. S. *J. Chem. Phys.* **1967**, *46*, 1694.

(33) Baldwin, R. R.; Keen, A.; Walker, R. W. *J. Chem. Soc., Faraday Trans. 2* **1987**, *83*, 759.

(34) Lin, M. C.; Laidler, K. J. *Can. J. Chem.* **1967**, *45*, 1315.

(35) (a) Gruver, J. T.; Calvert, J. G. *J. Am. Chem. Soc.* **1956**, *78*, 5208. (b) Calvert, J. G. *Chem. Rev.* **1959**, *59*, 569.

(36) Tedder, J. M.; Walton, J. C.; Winton, K. D. R. *J. Chem. Soc., Faraday Trans. 1* **1972**, *68*, 1866.

(37) Seakins, P. W.; Pilling, M. J.; Niiranen, J. T.; Gutman, D.; Krasnoperov, L. N. *J. Phys. Chem.* **1992**, *96*, 9847.

(38) Pedley, J. B.; Naylor, R. D.; Kirby, S. P. *Thermochemical Data of Organic Compounds*, 2nd ed.; Chapman and Hall: New York, 1986.

(39) Pedley, J. B. *Thermochemical data and structures of organic compounds*, v. 1; TRC Data Series; Texas A&M: College Station, TX, 1991.

(40) Russell, J. J.; Seetula, J. A.; Senkan, S. M.; Gutman, D. *Int. J. Chem. Kinet.* **1988**, *20*, 759.

(41) Dobis, O.; Benson, S. W. *Int. J. Chem. Kinet.* **1987**, *19*, 691.

(42) Pople, J. A.; Scott, A. P.; Wong, M. W.; Radom, L. *Isr. J. Chem.* **1993**, *33*, 345.

(43) Frisch, M. J.; Trucks, G. W.; Schlegel, H. B.; Gill, P. M. W.; Johnson, B. G.; Robb, M. A.; Cheeseman, J. R.; Keith, T.; Petersson, G. A.; Montgomery, J. A.; Raghavachari, K.; Al-Laham, M. A.; Zakrzewski, V. G.; Ortiz, J. V.; Foresman, J. B.; Cioslowski, J.; Stefanov, B. B.; Nanayakkara, A.; Challacombe, M.; Peng, C. Y.; Ayala, P. Y.; Chen, W.; Wong, M. W.; Andres, J. L.; Replogle, E. S.; Gomperts, R.; Martin, R. L.; Fox, D. J.; Binkley, J. S.; Defrees, D. J.; Baker, J.; Stewart, J. P.; Head-Gordon, M.; Gonzalez, C.; Pople, J. A. *Gaussian 94*, Revision E.1*;* Gaussian, Inc.: Pittsburgh, PA, 1995.

(44) Certain commercial instruments and materials are identified in this article to adequately specify the procedures. In no case does such identification imply recommendation or endorsement by NIST, nor does it imply that the instruments or materials are necessarily the best available for this purpose.

(45) Gang, J.; Robertson, S. H.; Pilling, M. J. *J. Chem. Soc., Faraday Trans.* **1997**, *93*, 1481.

(46) Knyazev, V. D.; Slagle, I. R. *J. Phys. Chem.* **1996**, *100*, 16899.

(47) Knyazev, V. D.; Bencsura, A.; Stoliarov, S. I.; Slagle, I. R. *J. Phys. Chem.* **1996**, *100*, 11346.

(48) Fukui, K. *Acc. Chem. Res.* **1981**, *14*, 363.

(49) Gonzalez, C.; Schlegel, H. B. *J. Phys. Chem.* **1990**, *94*, 5523.

(50) Eckart, C. *Phys. Rev.* **1930**, *35*, 1303.

(51) (a) Schlegel, H. B. *J. Chem. Phys.* **1986**, *84*, 4530. (b) Schlegel, H. B. *J. Phys. Chem.* **1988**, *92*, 3075.

(52) Johnston, H. S.; *Gas-Phase Reaction Rate Theory*; The Ronald Press: New York, 1966.

(53) Schranz, H. W.; Nordholm, S. *Chem. Phys.* **1984**, *87*, 163.

(54) Smith, S. C.; McEwan, M. J.; Gilbert, R. G. *J. Chem. Phys.* **1989,** *90*, 4265.

(55) Bernshtein, V.; Oref, I. *J. Phys. Chem.* **1993**, *97*, 6830.

(56) Kiefer, J. H.; Kumaran, S. S.; Sundaram, S. *J. Chem. Phys.* **1993,** *99*, 3531.
(57) Barker, J. R.; King, K. D. *J. Chem. Phys.* **1995,** *103*, 4953.
(58) Tsang, W.; Bedanov, V.; Zachariah, M. R. *J. Phys. Chem.* **1996**, *100*, 4011.
(59) Kiefer, J. H. *Symp. (Int.) Combust., [Proc.]* **1998**, *27*, 113.
(60) Wilkinson, J. H.; Reinsch, C. *Linear Algebra*; Springer: New York, 1971.
(61) Bedanov, V. M.; Tsang, W.; Zachariah, M. R. *J. Phys. Chem.* **1995**, *99*, 11452.
(62) Mokrushin, V.; Bedanov, V.; Tsang, W.; Zachariah, M. R.; Knyazev, V. D. *ChemRate, Version 1.16*; National Institute of Standards and Technology: Gaithersburg, MD 20899.
(63) Astholz, D. C.; Troe, J.; Wieters, W. *J. Chem. Phys.* **1979**, *70*, 5107.
(64) Knyazev, V. D. *J. Phys. Chem. A* **1998**, *102*, 3916.
(65) (a) Pitzer, K. S.; Gwinn, W. D. *J. Chem. Phys.* **1942**, *10*, 428. (b) Pitzer, K. S. *J. Chem. Phys.* **1946**, *14*, 239.
(66) Gang, J.; Robertson, S. H.; Pilling, M. J. *J. Chem. Soc., Faraday Trans.* **1996**, *92*, 3509.
(67) Miller, W. H. *J. Am. Chem. Soc.* **1979**, *101*, 6810.
(68) Kato, S.; Morokuma, K. *J. Chem. Phys.* **1980**, *72*, 206.
(69) Karas, A. J.; Gilbert, R. G.; Collins, M. A. *Chem. Phys. Lett.* **1992**, *193*, 181.
(70) Rabinovitch, B. S.; Tardy, D. C. *J. Chem. Phys.* **1966**, *45*, 3720.
(71) Chimbayo, A.; Toselli, B. M.; Barker, J. R. *J. Chem. Phys.* **1998**, *108*, 2383.
(72) Barker, J. R. *Ber. Bunsen-Ges. Phys. Chem.* **1997**, *101*, 566.
(73) (a) Hippler, H.; Troe, J. In *Bimolecular Reactions*; Ashfold, M. N. R., Baggott, J. E., Eds.; The Royal Society of Chemistry: London, 1989. (b) Oref, I.; Tardy, D. C. *Chem. Rev.* **1990**, *90*, 1407. (c) Barker, J. R.; Toselli, B. M. *Int. Rev. Phys. Chem.* **1993**, *12*, 305.
(74) Hold, U.; Lenzer, T.; Luther, K.; Reihs, K.; Symonds, A. *Ber. Bunsen-Ges. Phys. Chem.* **1997**, *101*, 552.
(75) Flynn, G. W.; Paramenter, C. S.; Wodtke, A. M. *J. Phys. Chem.* **1996**, *100*, 31.
(76) Knyazev, V. D. *J. Phys. Chem.* **1995**, *99*, 14738.
(77) Feng, Y.; Niiranen, J. T.; Bencsura, A.; Knyazev, V. D.; Gutman, D. *J. Phys. Chem.* **1993**, *97*, 871.
(78) Seakins, P. W.; Robertson, S. H.; Pilling, M. J.; Slagle, I. R.; Gmurczyk, G. W.; Bencsura, A.; Gutman, D.; Tsang, W. *J. Phys. Chem.* **1993**, *97*, 4450.
(79) Pittam, D. A.; Pilcher, G. *J. Chem. Soc., Faraday Trans. 1* **1972**, *68*, 2224.
(80) Gilbert, R. G.; Luther, K.; Troe, J. *Ber. Bunsen-Ges. Phys. Chem.* **1983**, *87*, 169.
(81) Venkatesh, P. K.; Dean, A. M.; Cohen, M. H.; Carr, R. W. *J. Chem. Phys.* **1999**, *111*, 8313.
(82) Heymann, M.; Hippler, H.; Troe, J. *J. Chem. Phys.* **1984**, *80*, 1853.
(83) Lim, K. F. *J. Chem. Phys.* **1994**, *101*, 8756.
(84) Dashevskaya, E. I.; Nikitin, E. E.; Oref, I. *J. Phys. Chem.* **1995**, *99*, 10797.
(85) (a) Boriesson, L.; Nordholm, S. *J. Phys. Chem.* **1995**, *99*, 938. (b) Boriesson, L.; Nordholm, S. *Chem. Phys.* **1996**, *212*, 393.
(86) Ming, L.; Sewell, T. D.; Nordholm, S. *Chem. Phys.* **1995**, *199*, 83.
(87) Lendvay, G.; Schatz, G. C. *J. Phys. Chem.* **1994**, *98*, 6530.
(88) Lenzer, T.; Luther, K.; Troe, J.; Gilbert, R. G.; Lim, K. F. *J. Chem. Phys.* **1995**, *103*, 626.
(89) Bernshtein, V.; Oref, I.; Lendvay, G. *J. Phys. Chem.* **1996**, *100*, 9738.
(90) (a) Hassoon, S.; Oref, I.; Steel, C. *J. Chem. Phys.* **1989**, *89*, 1743. (b) Morgulis, J. M.; Sapers, S. S.; Steel, C.; Oref, I. *J. Chem. Phys.* **1990**, *90*, 923.
(91) Barker, J. R. *Ber. Bunsen-Ges. Phys. Chem.* **1997**, *101*, 566.
(92) Tsang, W. *Combust. Flame* **1989**, *78*, 71.
(93) Vereecken, L.; Huyberechts, G.; Peeters, J. *J. Chem Phys.* **1997**, *106*, 6564.
(94) Venkatesh, P. K.; Dean, A. M.; Cohen, M. H.; Carr, R. W. *J. Chem. Phys.* **1997**, *107*, 8904.
(95) Frankcombe, T. J.; Smith, S. C.; Gates, K. E.; Robertson, S. H. *Phys. Chem. Chem. Phys.* **2000**, *2*, 793.